Title: A Proteomic Atlas of Senescence-Associated Secretomes for Aging Biomarker Development

Short Title: A Proteomic Atlas of the Senescence-Associated Secretory Phenotype

Authors: Nathan Basisty[1], Abhijit Kale[1], Okhee H Jeon[1], Chisaka Kuehnemann[1], Therese Payne[1], Chirag Rao[1], Anja Holtz[1], Samah Shah[1], Vagisha Sharma[3], Luigi Ferrucci[4], Judith Campisi[1, 2], Birgit Schilling**[1]

[1] The Buck Institute for Research on Aging, Novato, California 94947, USA.

[2] Lawrence Berkeley Laboratory, University of California, Berkeley, California 94720, USA.

[3] University of Washington, Seattle, Washington 98195, USA.

[4] National Institute on Aging, Bethesda, Maryland 20892, USA.

** Correspondence: bschilling@buckinstitute.org

Abstract

The senescence-associated secretory phenotype (SASP) has recently emerged as a driver of, and promising therapeutic target for, multiple age-related conditions, ranging from neurodegeneration to cancer. The complexity of the SASP, typically assessed by a few dozen secreted proteins, has been greatly underestimated, and a small set of factors cannot explain the diverse phenotypes it produces *in vivo*. Here, we present the 'SASP Atlas', a comprehensive proteomic database of soluble and exosome SASP factors originating from multiple senescence inducers and cell types. Each profile consists of hundreds of largely distinct proteins, but also includes a subset of proteins elevated in all SASPs. Our analyses identify several candidate biomarkers of cellular senescence that overlap with aging markers in human plasma, including GDF15, STC1 and SERPINs, which significantly correlated with age in plasma from a human cohort, the Baltimore Longitudinal Study of Aging. Our findings will facilitate the identification of proteins characteristic of senescence-associated phenotypes and catalog potential senescence biomarkers to assess the burden, originating stimulus and tissue of origin of senescent cells *in vivo*.

Abbreviations: ATV, atazanavir treatment; BLSA, Baltimore Longitudinal Study of Aging; CTL, control; DDA, data-dependent acquisition; DAMP, damage-associated molecular pattern; DIA, data-independent acquisition; eSASP, extracellular vesicle senescence associated secretory phenotype; EVs, extracellular vesicles; IR, X-irradiation; MS, mass spectrometry; RAS, inducible RAS overexpression; SA-β-Gal, senescence-associated β-galactosidase; SEN, senescent; sSASP, soluble senescence associated secretory phenotype**.**

Introduction

Cellular senescence is a complex stress response that causes an essentially irreversible arrest of cell proliferation and development of a multi-component senescence-associated secretory phenotype (SASP) [1–4]. The SASP consists of a myriad of cytokines, chemokines, growth factors and proteases that initiate inflammation, wound healing and growth responses in nearby cells [5,6]. In young healthy tissues, the SASP is typically transient and tends to contribute to the preservation or restoration of tissue homeostasis [5]. However, senescent cells increase with age and a chronic SASP is known or suspected to be a key driver of many pathological hallmarks of aging, including chronic inflammation, tumorigenesis and impaired stem cell renewal [5,7]. Powerful research tools have emerged to investigate the effect of senescence on aging and disease, including two transgenic $p16^{Ink4a}$ mouse models that allow the selective elimination of senescent cells [8,9] and compounds that mimic the effect of these transgenes. Data from several laboratories, including our own, strongly support the idea that senescent cells and the SASP drive multiple age-related phenotypes and pathologies, including atherosclerosis [10], osteoarthritis [11], cancer metastasis and cardiac dysfunction [12,13], myeloid skewing [14,15], kidney dysfunction [16], and overall decrements in healthspan [17]. Recently, senescent cells were shown to secrete bioactive factors into the blood that alter hemostasis and drive blood clotting [18]. SASP factors therefore hold potential as plasma biomarkers for aging and age-related diseases that are marked by the presence of senescent cells.

To develop robust and specific senescence and aging biomarkers, a comprehensive profile of the context-dependent and heterogeneous SASP is needed.

Several types of stress elicit a senescence and SASP response, which in turn can drive multiple phenotypes and pathologies associated with mammalian. These stressors have both shared and distinct secretory components and biological pathways. For example, telomere attrition resulting from repeated cell division (replicative senescence), ionizing radiation, chromatin disruption, and activation of certain oncogenes all can cause senescence-inducing genotoxic stresses, as can genotoxic therapeutic drugs, such as certain anti-cancer chemotherapies [13] and therapies for HIV treatment or prevention [19]. However, while both ionizing radiation and oncogenes lead to DNA double-strand breaks, ionizing radiation uniquely produces clustered oxidative DNA lesions [20] whereas oncogene activation drives DNA hyper-replication and double strand breaks [21]. Whether different senescence-inducers produce similar or distinct SASPs is at present poorly characterized. Thus, a comprehensive characterization of SASP components is critical to understanding how senescent responses can drive diverse pathological phenotypes *in vivo*.

The SASP was originally characterized by antibody arrays, which are necessarily biased, to measure the secretion of a small set of pro-inflammatory cytokines, proteases and protease inhibitors, and growth factors [1,2,4,22]. Subsequently, numerous unbiased gene expression studies performed on different tissues and donors of varying ages suggest that the SASP is more complex and heterogeneous [23], however, a recent meta-analysis of senescent cell transcriptomes confirmed the expression of a few dozen originally characterized SASP factors in multiple senescent cell types [24].

While unbiased transcriptome analyses are valuable, they do not directly assess the presence of *secreted* proteins. Thus, proteomic studies are needed to accurately

and quantitatively identify SASP factors as they are present in the secretomes of senescent cells. Recently, a mass spectrometric study reported several SASP factors induced by genotoxic stress [25], but an in-depth, quantitative and comparative assessment of SASPs originating from multiple stimuli and different cell types is lacking. Senescent cells also secrete bioactive exosomes [26,27] with both protein and miRNA [28] cargos. But, aside from pro-tumorigenic effects [28] and ability to induce paracrine senescence [26,29] , the proteomic content and function of exosomes and small extracellular vesicles (EVs) secreted by senescent cells remains largely unexplored.

In this study, we demonstrate that the SASP is not a single phenotype, but rather is highly complex, dynamic and dependent on the senescence inducer and cell type. Here we also present the "SASP Atlas" (www.SASPAtlas.com), a comprehensive, curated and expanding online database of the soluble secretomes of senescent cells (sSASPs) induced by various stimuli in several cell types. We also present the first comprehensive proteomic analysis of the exosomal SASP (eSASP), which is largely distinct from the sSASP. Our approach leverages an innovative data-independent mass spectrometry workflow to discover new SASP biomarker candidates. The SASP Atlas can help identify candidate biomarkers of aging and diseases driven by senescent cells. We also show that the SASP is enriched for protein markers of human aging and propose a panel of top SASP-based aging and senescence biomarker candidates.

Results

Cellular senescence entails extensive changes in the secreted proteome

We established an efficient, streamlined proteomic workflow to discover novel SASP factors. We collected proteins secreted by senescent and quiescent/control primary human lung fibroblasts (IMR90) and renal cortical epithelial cells (**Fig 1)**. Briefly, we induced senescence in the cultured cells by X-irradiation (IR), inducible oncogenic RAS overexpression (RAS), or treatment with the protease inhibitor atazanavir (ATV, used in HIV treatment) and allowed 1-2 weeks for the senescent phenotype to develop, as described [2]. In parallel, control cells were made quiescent by incubation in 0.2% serum for 3 days and were either mock-irradiated or vehicle-treated. Treated and control cells were subsequently cultured in serum-free medium for 24 hours and the conditioned media, containing soluble proteins and exosomes/extracellular vesicles (EVs), was collected. Soluble proteins and exosomes/EVs were separated by ultracentrifugation.

The label-free data-independent acquisition (DIA) approach enabled sensitive and accurate quantification of SASP proteins by integrating the MS2 fragment ion chromatograms [30,31]. We quantitatively compared proteins secreted by senescent cells with controls, and significantly changed proteins (q-value <0.05) that had a fold change of at least 1.5-fold (SEN/CTL) were identified. Proteins secreted at significantly higher levels by senescent relative to quiescent cells were defined as SASP factors. In fact, most proteins were secreted at much higher levels by senescent cells compared to non-senescent cells (**Fig 2**). Each treatment and control group contained 4-10 biological replicates (see Methods for replicate details and experimental design). Relative protein quantification and statistical details are presented in **Table S1**.

Induction of senescence was verified by senescence-associated β-galactosidase (SA-β-

Gal) activity and p16INK4a and IL-6 mRNA levels (**Fig S1A-C**), as described [2]. There was no detectable cell death, as measured by a Sytox Green viability dye assay (**Fig S2**). X-irradiation and RAS overexpression induced senescence in >90% of cells and ATV induced senescence in about 65% of cells (**Fig S1A-B**).

Fig 1. Proteomic workflow for isolation and analysis of secreted proteins and exosomes/EVs. Senescence was induced in cultured primary human lung fibroblasts and renal epithelial cells by either X-irradiation (IR), inducible oncogenic RAS overexpression (RAS), or atazanavir (ATV). Control cells were made quiescent and either mock irradiated or vehicle treated. Soluble proteins and exosomes/EVs were then isolated from conditioned media. Samples were digested and subjected to mass spectrometric analysis (DIA), followed by protein identification and quantification using Spectronaut Pulsar [32] and by bioinformatic, pathway and network analyses in R and Cytoscape [33,34]. SEN = Senescent, CTL = Control.

This unbiased proteomic profiling identified up to ~1700 secreted proteins, a large fraction of which were up- or down-regulated following induction of senescence by IR, RAS or ATV (**Fig 2**). Between 340 to 714 proteins changed significantly in response to each inducer. As expected, most of the significantly changed proteins were markedly upregulated in senescent, compared to quiescent, cells, but, interestingly, a minority were downregulated (**Fig 2A**). Notably, the protein cargo of exosomes/EVs released by senescent cells was distinct compared to that from non-senescent cells (**Fig 2A**), indicating the existence of an exosome/EV SASP (eSASP) in addition to the sSASP.

Fig 2. Core sSASP proteins, networks and pathways. (A) Summary of proteins with significantly altered (q-value<0.05) secretion by senescent compared to quiescent cells following genotoxic, oncogenic, or ATV treatment stress in senescent human lung fibroblasts and renal epithelial cells. B) Venn diagram of proteins showing significantly increased secretion in senescent versus non-senescent cells following induction of senescence by IR, RAS or ATV. (C) ClueGO [33] pathway enrichment and network analyses of overlapping sSASPs resulting from each senescence inducer. Pathways of the same color have >= 50% similarity. Connecting lines represent Kappa connectivity scores >40%. (D) Secretion levels of proteins in the neurodegeneration pathway, expressed as log2 fold change of senescent versus control cells. (E) Unsupervised K-means clustering of proteins significantly increased in the sSASPs of all inducers based on the magnitude of the protein changes (log2-change) in senescent versus control groups and partitioned into three clusters. IR = X-irradiation, RAS = RAS oncogene overexpression, ATV = atazanavir treatment.

Most changes in the sSASP, independent of inducer, exhibited increased secretion by senescent cells, with only 1-6% of proteins secreted at lower levels. In contrast, one-half to two-thirds of all significant protein changes in exosomes/EVs from senescent fibroblasts were decreased relative to quiescent cells (**Fig 2A**). For renal epithelial cells, the sSASP comprised a more even mix of proteins with significantly lower or higher relative secretion. The magnitude of the fold-changes in the sSASP were generally higher in fibroblasts than in renal epithelial cells, regardless of inducer

(**Fig 2A**). For example, 531 of significant protein changes in the fibroblast sSASP were >2-fold, compared to 138 in the renal epithelial cell sSASP. However, for renal epithelial cells an additional 212 proteins showed significant changes between 1.5- and 2-fold increase or decrease.

For each cell type and fraction, we also measured the secretion of known SASP factors (**Fig S1D**). These factors included chemokines (CXCLs), high mobility group box 1 protein (HMGB1), IGF binding proteins (IGFBPs), matrix metalloproteinases (MMPs), lamin B1 (LMNB1), and tissue inhibitors of metallopeptidase (TIMPs). In fibroblasts, all previously identified SASP factors were elevated, regardless of the senescence inducer. However, while expression of p16INK4a, IL-6 and SA-β-Gal were also elevated in renal epithelial cells (**Fig S1A-C**), most classical SASP proteins were either decreased or unchanged, except for IGFBP2. This finding suggests that fibroblast SASP markers do not necessarily pertain to other cell types. Similarly, within exosomes/EVs secreted by senescent fibroblasts, nearly all previously identified key SASP factors were either absent, unchanged or decreased, and none were consistently elevated in response to more than one inducer (**Fig S1D**).

Senescence-inducing stimuli drive largely distinct secretory phenotypes

To determine how different senescence-inducing stimuli affect the SASPs, we compared the sSASP from human primary fibroblasts induced to senesce by IR, RAS or ATV. Strikingly, the sSASP was largely distinct among inducers, with an overlap of 150 proteins among 1091 total increased proteins and no overlap among decreased

proteins (**Table S2**). Thus, most SASP protein components and corresponding changes were highly heterogenous and not shared among inducers (**Fig 2B**).

To determine whether there are core pathways associated with the SASPs, we performed pathway and network analyses on overlapping proteins in the sSASPs of each inducer (**Fig 2C**). The largest pathway associated with all inducers related to tissue and cell structure, including extracellular matrix, cytoskeleton, integrins and peptidase activity. Interestingly, neurodegeneration and three related pathways with high agreement (kappa score >40%) – apoptosis, ROS signaling and TP53-regulated metabolism - were also enriched among the overlapping sSASP proteins (**Fig 2C-D**). Among the neurodegeneration proteins were amyloid precursor protein (APP) and cystatin 3 (CST3), related to Alzheimer's pathogenesis and risk [35,36], as well as Parkinsonism-associated deglycase (PARK7 or DJ1) [37] (**Fig 2D**). This enrichment of neurodegeneration-associated proteins and pathways suggests that senescent cells contribute to neurodegenerative diseases, for which these sSASP factors might serve as biomarkers, regardless of the senescence-inducing stimuli.

To distill the overlapping 'core' sSASP proteins into primary components, we performed an unsupervised machine learning analysis (**Fig 2E**). K-means clustering analysis uncovered three primary clusters among core sSASP components. Strikingly, one cluster, consisting of just three proteins – chemokine C-X-C motif ligand 1 (CXCL1), matrix metallopeptidase 1 (MMP1), and stanniocalcin 1 (STC1) – were highly represented in the sSASPs of all inducers, suggesting these proteins might serve as surrogate markers of the sSASP. Of note, STC1, among the top sSASP proteins, is a

220 previously unidentified SASP factor and a secreted hormone with many disease
221 associations [38–43]. Our analyses also validate MMP1 and CXCL1 as SASP markers.
222
223 **sSASP is largely distinct in composition and regulation in fibroblasts and**
224 **epithelial cells**
225 We compared the secretomes of lung fibroblasts and renal epithelial cells to
226 determine the cell-type specificity of the sSASP. The sSASP of these cells were largely
227 distinct (**Fig 3A-B**). Among the proteins increased in the sSASP of each cell type, 9-
228 23% overlapped, and the magnitude of the changes by renal epithelial cells were, in
229 most cases, lower than in fibroblasts regardless of the senescence inducer, although it
230 is possible that senescent fibroblasts secrete more protein overall than epithelial cells in
231 response to stress. Interestingly, 20-30% of proteins significantly decreased in the
232 sSASP of renal epithelial cells overlapped with proteins significantly increased in the
233 fibroblast sSASP (**Fig 4B**). Among the epithelial factors that changed oppositely to the
234 fibroblast factors were IGFBPs, TIMPs 1 and 2, CXCL1 and most SERPINs (**Fig 2C**). In
235 all, 17 sSASP factors were shared between all senescence inducers and cell types we
236 examined (**Table S3**).
237
238 **Fig 3. Epithelial cells and fibroblasts have distinct sSASPs. (**A) Venn diagram
239 comparing proteins significantly increased in the sSASPs of senescent fibroblasts and
240 epithelial cells, both induced by X-irradiation ($q < 0.05$). (B) Venn diagram comparing
241 protein increases in the fibroblast sSASP vs *decreases* in the epithelial sSASP. (C)
242 Pathway and network analysis of secreted proteins significantly increased by senescent

fibroblasts and epithelial cells. (D) Pathway and network analysis of proteins significantly increased in the fibroblast sSASP but significantly decreased in the epithelial cell sSASP.

Pathway and network analysis of proteins increased in the sSASPs of fibroblasts and epithelial cells (**Fig 3C**) showed that most pathways belonged to one of three general categories: protein turnover and secretion, primary metabolism, and cellular detoxification. While not as apparent on a molecule-by-molecule basis, many pathways were commonly enriched in both the epithelial and fibroblast sSASPs (**Fig 3C** and **Fig 2C**), including vesicle-mediated transport and exosomes, glycolytic metabolism, and cellular detoxification. Of notable exceptions, pathways enriched uniquely by epithelial cells included protein translation and degradation (lysosome and phagosome).

Surprisingly, most renal epithelial sSASP proteins with significantly *lower* secretion by senescent cells were enriched in pathways related to tissue and cell structure, adhesion and motility (**Fig 3D**). This finding contrasts with previous reports and our own analyses of fibroblasts (**Fig 2C**), in which these pathways were increased, regardless of inducer. The irradiated epithelial sSASP also had significantly lower levels of proteins involved in RNA processing, in contrast to increased RNA metabolism in the irradiated fibroblast sSASP. Additionally, the epithelial sSASP was significantly depleted in proteins related to proteasome degradation, antigen processing and the complement system.

Damage-associated molecular patterns (DAMPs, also known as alarmins or danger signals) are released from cells in response to internal and external stress, and

266 are components of the SASP [44]. HMGB1 is a founding member of the DAMPs, a
267 prominent SASP marker, and, along with calreticulin (CALR), an important driver of
268 inflammation [44]. Our analysis identified increased secretion of multiple DAMPs,
269 including HMGB1 and CALR, by senescent fibroblasts under all senescence inducers
270 (**Table 1**). However, the secretion of DAMPs was unchanged or significantly reduced
271 by senescent epithelial cells, demonstrating that some defining SASP components vary
272 depending on cell type.

273

274 **Table 1: DAMPs are a core component of the fibroblast sSASP**

275

Log2(SEN/CTL)

	IR (Fibroblasts)	RAS	ATV	IR (Epithelial)
HMGB1	2.47	0.59	2.46	NS
CALR	1.22	0.51	1.32	-1.00
CD44	2.25	1.20	1.92	-0.69
S100A11	0.56	1.35	1.88	NS
LGALS3BP	1.46	1.76	1.79	-1.19
VCAN	1.80	1.32	0.98	-1.42
TNC	1.64	1.40	2.46	0.29
HSPA5	2.03	3.93	1.78	-0.34
HSP90AB1	5.01	2.69	1.65	NS
HSPA8	2.49	2.98	1.46	0.32
HSPA1A	2.96	2.4	1.45	0.54

HSP90AA1	4.94	3.42	1.34	NS
HSP90B1	2.67	1.61	0.66	-0.27

All changes are significant ($q < 0.05$) unless denoted NS (Not Significant). SEN = Senescent, CTL = Quiescent Control, IR = X-irradiation, RAS = oncogenic RAS overexpression, ATV = Atazanavir treatment.

Exosome/EV proteomic signatures are altered by cellular senescence.

Because proteins are also secreted as extracellular vesicle cargo, we hypothesized that senescent cells would show significant changes in this fraction, which we term the exosome/EV SASP (eSASP). We used ultracentrifugation to enrich conditioned media for exosomes and small EVs released by quiescent and senescent fibroblasts induced by X-irradiation and oncogenic RAS overexpression (**Fig 1**). We confirmed the quality of exosome/EV purified fractions by measuring presence of multiple EV-specific markers, including CD63 and CD9 [45], and by particle counting and size distribution analysis (**Fig S4**). Exosomes/EVs from senescent fibroblasts showed a strikingly altered protein composition compared with exosomes from non-senescent cells (**Fig 2A**).

To determine whether the characteristics of exosomes/EVs from senescent cells are altered, we analyzed particle number and size distribution of exosomes/EVs secreted into the culture medium of senescent and non-senescent cells over a 24-hour period. On average, senescent cells released a greater number of vesicles -- about 68 per cell compared to 49 per control cell (**Fig S4B**). However, the mean diameter, size distribution of senescent and control exosomes/EVs were similar (**Fig S4B-C**). Further

297 work using senolytics may validate whether the number, size, and other characteristics
298 of secreted exosome/EVs are indicators of senescent cell burdens in humans.

299 The protein content of exosomes/EVs released by IR- vs RAS-induced
300 senescent fibroblasts was largely distinct, sharing only 9 significantly altered proteins
301 (**Fig 4A**). Exosomes/EVs were reported to contain protein signatures of their originating
302 cells [28,46], offering a unique opportunity to identify senescence biomarkers with a
303 degree of cell type specificity. Thus, exosome/EV proteins might distinguish senescent
304 cells of different origins or resulting from different stressors. The membranes of
305 exosomes are also representative of the originating cells [28,46]. Indeed, about 30% of
306 all the exosome/EV proteins that increased upon senescence are plasma membrane
307 proteins (**Fig 4B**), suggesting that exosomes/EVs might also identify cell type origins
308 through their cell-surface proteins. In addition to enrichment of proteins involved in
309 membrane organization, such as cell adhesion and cell junction assembly proteins, the
310 eSASP is uniquely enriched with signaling pathways not found in the sSASP, such as
311 RAS signaling, G-protein signaling, and prostaglandin synthesis and regulation (**Fig**
312 **4C**). Full lists of proteins secreted by senescent exosomes are in **Table S1**.
313

314 **Fig 4. Cellular senescence alters exosome/EV features and composition.** (A)
315 Table showing overlapping significant protein changes in exosomes/EVs secreted by
316 senescent cells induced by IR vs RAS ($q < 0.05$). (B) Enrichment analysis of gene-
317 ontology/cellular compartments overrepresented among protein contents of
318 exosomes/EVs released by senescent cells. (C) Network analysis of pathways and
319 functions unique to the eSASP.

The SASP contains potential aging and disease biomarkers

As a driver of many aging and disease phenotypes, the SASP could include known biomarkers of aging and age-related diseases. A recent biomarker study identified 217 proteins that are significantly associated with age in human plasma (adjusted $p<0.00005$) [47]. Of these, 20 proteins (9.2%) were present in the originally-defined SASP [2]. Strikingly, multiple newly identified SASP factors from our present study were also identified in the study of human plasma [47] (**Fig 5**). Of all the originally-defined SASP factors and unique SASP proteins that we identify here, 101 proteins were also identified as markers of aging in human plasma (46.5% of all plasma aging markers) (**Fig 5A, C-D, Table S4**). Considering the originally defined SASP in addition our newly identified "core SASP" (SASP components resulting from all senescence inducers), the number of age-associated plasma proteins that are also SASP proteins is 40, or 18.4% of plasma aging markers (**Fig 5B-D**, **Table S4**). Thus, plasma biomarkers of aging are highly enriched with SASP factors.

Fig 5. Human plasma aging markers are enriched for SASP proteins. (A) Venn diagram comparing SASP factors secreted by at least one of IR- , RAS-, or ATV-induced senescent cells with markers of aging identified in human plasma [47]. (B) Overlap between the core SASP (proteins secreted following all senescence-inducing stimuli) and plasma aging markers. (C) Pie chart showing the proportion of known SASP factors, newly identified core SASP factors, and SASP factors found among plasma markers of aging in humans. (D) Number of proteins contained in the originally

identified SASP, core SASP, non-core SASP, and markers of aging in human plasma [47] ($p<0.00005$). Top core SASP factors GDF15, STC1, SERPINs, and MMP1 are among the plasma aging markers.

Complement and coagulation cascade proteins [18], particularly protease inhibitors such as SERPINs, were also noted as prominent plasma biomarkers of aging [47]. These proteins and their pathway networks were robustly altered in the SASPs of cells induced to senesce by all the tested stressors (**Fig 2C, Fig 6A**). The protein having the strongest association with aging [47], GDF15 ($r=0.82$), was among the most highly secreted proteins in the sSASP induced by IR, RAS and ATV in fibroblasts, and in epithelial cells induced by IR (**Fig 6D**). Increased secretion of top core SASP biomarkers SERPINE1, MMP1, STC1, and GDF15 was confirmed by western blotting in RAS-induced senescent cells compared to controls (**Fig S3**). The enrichment of aging and disease biomarkers in the secretomes of senescent cells supports their link to a wide spectrum of age-related diseases.

Fig 6. The SASP contains aging and disease biomarkers. (A) Serpins are secreted at high levels by senescent fibroblasts induced by IR, RAS or ATV. (B) MMP1 and (C) STC1 are among the most highly secreted proteins by senescent fibroblasts. (D) The plasma aging biomarker GDF15 is increased in the sSASPs of fibroblasts induced to senesce by IR, RAS and ATV and epithelial cells induced to by IR. IR = X-irradiation, RAS = RAS oncogene overexpression, ATV = atazanavir treatment, Epi = renal epithelial cells. *$q < 0.05$, **$q < 0.01$, ***$q < 0.001$.

Discussion

Here we present SASP Atlas (www.SASPAtlas.com), the first proteome-based database of SASPs. This database contains the contents of exosome/EV and soluble secretomes, in addition to SASPs originating from multiple senescence-inducing stresses and two distinct cell types. The SASP Atlas will be continuously updated with SASP profiles from new cell types and senescence, including paracrine (or bystander) senescence [48,49], as well as temporal dynamics of the SASP – all generated by our laboratories.

Our proteomic analysis leverages a modern data-independent acquisition (DIA or SWATH) mass spectrometry workflow, which comprehensively acquires label-free, quantitative peptide (MS1) and fragment-level (MS2) data for all peptides in each sample [30–32,50,51]. DIA workflows are not limited by the stochastic peptide MS/MS sampling biases characteristic of traditional data-dependent acquisition (DDA) mass spectrometry. In addition to the SASP Atlas database, we provide panels of SASP factors on Panorama Web, a freely-available web repository for targeted mass spectrometry assays [52,53]. These resources can be used as a reference and guide to identify and quantify SASP factors that may be associated with specific diseases, and to develop aging and disease-related biomarkers (**Fig 7**).

Fig 7. SASP Atlas: A Comprehensive Resource for Senescence-Associated Secretory Phenotypes. SASP Atlas (www.SASPAtlas.com) is a curated and freely-available database of the secretomes of senescent cells, including both the soluble and

389 exosome SASP, that can be used to identify SASP components or biomarker
390 candidates for senescence burden, aging and related diseases.
391
392 SASP profiles are needed to develop senescence biomarkers in human plasma
393 or other biofluids, and for identifying individuals to treat with, and measuring the efficacy
394 of, senescence-targeted therapies such as senolytics. Translating senescence- and
395 SASP-targeted interventions to humans will require a comprehensive profile of SASPs,
396 both to identify their deleterious components and to develop human biomarkers to
397 assess senescent cell burden. The SASP, as originally identified, comprised ~50
398 cytokines, chemokines, growth factors, and proteases that were detected by biased
399 methods (e.g., antibody arrays) and/or transcriptional analyses [1–4,24]. While these
400 comprehensive analyses are valuable in describing the overall phenotype of senescent
401 cells, proteomic analyses are complimentary in both confirming transcriptional changes
402 and identifying and quantifying novel SASP factors that are not apparent at the mRNA
403 level. For example, a recent meta-analysis of senescent cell transcriptomes [24]
404 identified >1,000 genes with increased expression specifically in senescent cells
405 induced by IR or oncogenic RAS, and >700 'core' senescence genes (increased
406 expression following all senescence inducers tested). Our analysis identified 548, 644,
407 and 143 proteins in the IR, RAS and 'core' SASP, respectively, that were previously
408 unreported at the RNA level (**Fig S5**). We expect that the number and nature of these
409 SASP core proteins will change as we and others interrogate additional cell types and
410 senescence inducers, and we will continue to curate the interactive SASP Atlas.

411 Additionally, the secretion of SASP factors, such as HMGB1 and other DAMPs, is not
412 generally transcriptionally driven.

413 DAMP receptor-bearing cells, including cells of the innate immune system,
414 recognize extracellular DAMPs as signals to promote inflammatory and fibrotic
415 responses. Increased circulating DAMPs are hypothesized to play a role in aging
416 [54,55], particularly the age-related inflammation termed 'inflammaging' [56]. DAMPs
417 can also serve as biomarkers of a number of diseases, including trauma and
418 cardiovascular, metabolic, neurodegenerative, malignant and infectious diseases
419 [54,57,58]. In addition, our top "core sSASP" biomarker candidates, have been
420 identified as disease biomarkers in human studies. For example, human cohort studies
421 have recently reported GDF15 as a biomarker of cardiovascular disease, cardiovascular
422 and cancer mortality and morbidity, renal disease, and all-cause mortality independent
423 of cardiovascular mortality [59–65]. Additionally, two of the top "core sSASP" proteins
424 identified by an unbiased k-means clustering algorithm – STC1 and MMP1 (**Fig 5C-D**) –
425 were reported as significant aging biomarkers [47]. In addition to aging, MMP1 has
426 been identified as a biomarker for several cancers, pulmonary fibrosis and potentially
427 Alzheimer's disease [66–69], whereas STC1 has been identified as a diagnostic and
428 prognostic biomarker for cancers, pulmonary fibrosis, renal ischemia/reperfusion injury
429 and Alzheimer's disease [38–43].

430 Our quantitative unbiased *proteomic* analysis of senescent fibroblasts and
431 epithelial cells reveals a much larger and diverse SASP than initially reported. These
432 SASP profiles contribute a number of new potential senescence, aging and disease
433 biomarkers. In addition to general senescence biomarkers, many proteins will likely be

specific to cell-type and originating stimulus. Thus, biomarkers present in human patients *in vivo* will likely vary depending on the affected tissue, originating cell types, and senescence stimuli. Therefore, comprehensive quantitative profiles of the SASP under a variety of physiological conditions will provide biomarker candidates with a higher degree of selectivity to specific pathologies in humans.

Materials and Methods

Reagents and Resources

A full list of reagents and resources, including vendors and catalog numbers, are available in a Reagent and Resource Table (**Table S5**). Further information and requests for resources and reagents should be directed to the Lead Contact, Birgit Schilling (bschilling@buckinstitute.org).

Human Cell Culture and Primary Cell Lines

IMR-90 primary human lung fibroblasts (ATCC #CCL-186) were cultured in Dulbecco's Modified Eagle's Medium (DMEM, Gibco #12430-054) supplemented with penicillin and streptomycin (5000 U/mL and 5000 μg/mL, Gibco #15070063) and 10% Fetal Bovine Serum (FBS, Gibco #2614079). Primary human renal epithelial cells (ATCC PCS400011) were cultured in Renal Epithelial Cell Basal Medium (Female, ATCC #PCS-400-030). Both cell types were maintained at 37° C, 10% CO_2 and 3% O_2.

Induction of Senescence

X-irradiation: Senescence was induced by ionizing radiation (IR;10 Gy X-ray). Quiescent control cells were mock irradiated. Senescent cells were cultured for 10 days to allow development of the senescent phenotype, and quiescent cells were cultured in 0.2% serum for 3 days. Cells were then washed with PBS (Gibco #10010-023) and placed in serum- and phenol red-free DMEM (Gibco #21063-029) and conditioned media was collected after 24 hours.

RAS overexpression: RAS^{v12} was cloned in pLVX vector (Lenti-X™ Tet-On from Clontech #632162) to make inducible lentiviruses, which were used to infect early passage IMR-90 cells (PD-30). Transduced cells were selected in puromycin (1 µg/ml) for 24 hours. For induction of RAS^{v12}, cells were treated with 1 µg/ml doxycycline in DMSO (Sigma # D9891) for 4 (early time point) or 7 days. Doxycycline was replaced after every 48 hours. Subsequently, cells were washed with PBS and placed in serum- and phenol red-free DMEM and conditioned media was collected after 24 hours.

Atazanivir treatment: Cells were cultured in appropriate media containing 20 µM Atazanavir, which is a clinically relevant dose, or vehicle (DMSO) for 9 (early timepoint) or 14 days. Subsequently, cells were washed with PBS and placed in serum- and phenol red-free DMEM and conditioned media was collected after 24 hours.

Isolation of Secreted Soluble Proteins and Exosomes/EVs:

Proteins secreted into serum-free medium over a 24-hr period were collected. An ultracentrifugation protocol was used to separate the exosome and small extracellular vesicle fraction from the soluble protein fraction [70]. Briefly, conditioned medium was centrifuged at 10,000 x g at 4° C for 30 minutes to remove debris. The supernatant was

then centrifuged at 20,000 x g at 4° C for 70 minutes to remove microvesicles followed by ultracentrifugation at 100,000 x g at 4° C for 70 minutes to pellet exosomes. The exosome-depleted supernatant was saved as the sSASP. The exosome pellet was then washed twice with PBS and ultracentrifuged again at 100,000 x g at 4° C for 70 minutes before resuspending in PBS and saved as the eSASP.

Proteomic Sample Preparation

Chemicals: Acetonitrile (#AH015) and water (#AH365) were from Burdick & Jackson. Iodoacetamide (IAA, #I1149), dithiothreitol (DTT, #D9779), formic acid (FA, #94318-50ML-F), and triethylammonium bicarbonate buffer 1.0 M, pH 8.5 (#T7408) were from Sigma Aldrich, urea (#29700) was from Thermo Scientific, sequencing grade trypsin (#V5113) was from Promega and HLB Oasis SPE cartridges (#186003908) were from Waters.

Protein concentration and quantification: Samples were concentrated using Amicon Ultra-15 Centrifugal Filter Units with a 3 kDa cutoff (MilliporeSigma #UFC900324) as per the manufacturer instructions and transferred into 8M urea/50 mM triethylammonium bicarbonate buffer at pH 8. Protein quantitation was performed using a BCA Protein Assay Kit (Pierce #23225).

Digestion: Aliquots of each sample containing 25-100 µg protein were brought to equal volumes with 50 mM triethylammonium bicarbonate buffer at pH 8. The mixtures were reduced with 20 mM DTT (37°C for 1 hour), then alkylated with 40 mM iodoacetamide (30 minutes at RT in the dark). Samples were diluted 10-fold with 50 mM

501 triethylammonium bicarbonate buffer at pH 8 and incubated overnight at 37°C with
502 sequencing grade trypsin (Promega) at a 1:50 enzyme:substrate ratio (wt/wt).
503 Desalting: Peptide supernatants were collected and desalted with Oasis HLB 30 mg
504 Sorbent Cartridges (Waters #186003908, Milford, MA), concentrated, and re-suspended
505 in a solution containing mass spectrometric 'Hyper Reaction Monitoring' retention time
506 peptide standards (HRM, Biognosys #Kit-3003) and 0.2% formic acid in water.
507
508 **Mass Spectrometry Analysis**
509 Samples were analyzed by reverse-phase HPLC-ESI-MS/MS using the Eksigent Ultra
510 Plus nano-LC 2D HPLC system (Dublin, CA) combined with a cHiPLC system directly
511 connected to an orthogonal quadrupole time-of-flight SCIEX TripleTOF 6600 or a
512 TripleTOF 5600 mass spectrometer (SCIEX, Redwood City, CA). Typically, mass
513 resolution in precursor scans was ~ 45,000 (TripleTOF 6600), while fragment ion
514 resolution was ~15,000 in 'high sensitivity' product ion scan mode. After injection,
515 peptide mixtures were transferred onto a C18 pre-column chip (200 µm x 6 mm
516 ChromXP C18-CL chip, 3 µm, 300 Å, SCIEX) and washed at 2 µl/min for 10 min with
517 the loading solvent (H_2O/0.1% formic acid) for desalting. Peptides were transferred to
518 the 75 µm x 15 cm ChromXP C18-CL chip, 3 µm, 300 Å, (SCIEX), and eluted at 300
519 nL/min with a 3 h gradient using aqueous and acetonitrile solvent buffers.
520 All samples were analyzed by data-independent acquisitions (DIA), specifically using
521 variable window DIA acquisitions [71]. In these DIA acquisitions, windows of variable
522 width (5 to 90 m/z) are passed in incremental steps over the full mass range (m/z 400-
523 1250). The cycle time of 3.2 sec includes a 250 msec precursor ion scan followed by

524 45 msec accumulation time for each of the 64 DIA segments. The variable windows
525 were determined according to the complexity of the typical MS1 ion current observed
526 within a certain m/z range using a SCIEX 'variable window calculator' algorithm (more
527 narrow windows were chosen in 'busy' m/z ranges, wide windows in m/z ranges with
528 few eluting precursor ions) [31]. DIA tandem mass spectra produce complex MS/MS
529 spectra, which are a composite of all the analytes within each selected Q1 m/z window.
530 All collected data was processed in Spectronaut using a pan-human library that
531 provides quantitative DIA assays for ~10,000 human proteins [72].
532
533 **Cell Viability Assays**
534 Cell viability was assessed with SYTOX Green Nucleic Acid Stain (Invitrogen #S7020).
535 Senescent and control cells were incubated for 24 hours in serum-free medium
536 containing SYTOX Green with continuous imaging. Cell death was quantified by
537 counting total SYTOX Green positive nuclei during the 24-hour time-lapse video.
538
539 **Senescence-Associated β-Galactosidase Staining**
540 Senescence-associated beta-galactosidase (SA-β-gal) activity was determined using
541 the BioVision Senescence Detection Kit (Cat# K320-250). For each experiment,
542 approximately 100–150 cells were counted.
543
544 **RNA Extraction and Quantitative Real-Time PCR**
545 Total RNA was prepared using the PureLink Micro-to-Midi total RNA Purification System
546 (Invitrogen # 12183018A), according to the manufacturer's protocol. Samples were first

547 treated with DNase I Amp Grade (Invitrogen #18068015) to eliminate genomic DNA
548 contamination. RNA was reverse transcribed into cDNA using a High-Capacity cDNA
549 Reverse Transcription Kit (Applied Biosystems #4368813), according to the
550 manufacturer's protocol. Quantitative RT-PCR (qRT-PCR) reactions were performed as
551 described using the Universal Probe Library system (Roche). Actin and tubulin
552 predeveloped TaqMan assays (Applied Biosystems) were used to control for cDNA
553 quantity. qRT-PCR assays were performed on the LightCycler 480 System (Roche).
554 The primers and probes were as follows:
555 Human actin F 5'- CCAACCGCGAGAAGATGA; R 5'- TCCATCACGATGCCAGTG,
556 UPL probe #64
557 Human tubulin F 5'- CTTCGTCTCCGCCATCAG; R 5'- TTGCCAATCTGGACACCA,
558 UPL Probe #58
559 Human IL-6 F 5'- GCCCAGCTATGAACTCCTTCT; R 5'- GAAGGCAGCAGGCAACAC,
560 UPL Probe #45
561 Human $p16^{INK4a}$ F 5'-GAGCAGCATGGAGCCTTC; R 5'-CGTAACTATTCGGTGCGTTG,
562 UPL Probe #34
563

564 **Exosome Characterization and Size Distribution Analysis**

565 Protein determination is performed on exosomes/EVs isolated by ultracentrifugation by
566 direct absorbance and 20 µg of protein is used for input for the MacsPlex Exosome Kit
567 (Miltenyi) assay. These exosomes are enriched for CD63, CD9, and CD81 surface
568 proteins using antibody beads. This pool of exosomes is then probed for 34 other
569 surface markers used for analysis and comparison across samples. Particle diameter

and concentration were assessed by tunable resistive pulse sensing (TRPS) on an IZON qNano Nanoparticle Characterization instrument using a NP150 nanopore membrane at a 47 calibration with 110 nm carboxylated polystyrene beads at a concentration of 1.2x10^13 particles/mL (Zen-bio, Inc.).

Processing, Quantification, and Statistical Analysis of MS Data

DIA acquisitions were quantitatively processed using the proprietary Spectronaut v12 (12.020491.3.1543) software [32] from Biognosys. A pan-human spectral library was used for Spectronaut processing of the DIA data [72]. Quantitative DIA MS2 data analysis was based on extracted ion chromatograms (XICs) of 6-10 of the most abundant fragment ions in the identified spectra. Relative quantification was performed comparing different conditions (senescent versus control) to assess fold changes. The number of replicates for each experiment are as follows: X-irradiated fibroblasts, 4 senescent and 4 control replicates; X-irradiated epithelial cells, 5 senescent and 5 control replicates; 4 day RAS-induction fibroblasts, 10 senescent and 10 control replicates; 7 day RAS-induced fibroblasts, 6 senescent and 6 control replicates; atazanavir-treated fibroblasts, 3 senescent (9 days treatment), 3 senescent (14 days treatment), and 4 control replicates; X-irradiated fibroblast exosomes, 5 senescent and 5 control replicates; 7 day RAS-induced fibroblast exosomes, 6 senescent and 6 control replicates. Significance was assessed using FDR corrected q-values<0.05.

Pathway and Network Analysis

Gene ontology, pathway, and network analysis was performed using the GlueGO package, version 2.5.3, in Cytoscape, version 3.7.1 [33,34]. Curated pathways for enrichment analysis were referenced from the following databases: GO Biological Function, GO Cellular Compartment, Kegg pathways, WikiPathways, and Reactome Pathways. For gene ontology data, testing was restricted to pathways with experimental evidence (EXP, IDA, IPI, IMP, IGI, IEP). The statistical cutoff for enriched pathways was Bonferroni-adjusted p-values < 0.01 by right-sided hypergeometric testing. Pathway-connecting edges were drawn for kappa scores > 40%. Kappa scores are a measure of inter-pathway agreement among observed proteins that indicate whether pathway agreement is greater than expected by chance based on shared proteins. Pathways with the same color indicate >= 50% similarity in terms.

K-Means Clustering

Unsupervised clustering was performed in Python with Scikit-learn, a module integrating a wide range of machine learning algorithms [73]. Datasets were pre-processed with the StandardScaler function and clustered with the KMeans algorithm.

Data Visualization

Heatmaps were visualized in R using the heatmap.2 function in the ‘gplots’ package [74]. Venn diagrams were constructed using the “VennDiagram” package [75]. Color palettes in R were generated with the “RColorBrewer” package [76]. Pathway and network visualizations were generated and modified using the GlueGO package in Cytoscape [33,34].

Data availability: All raw files are uploaded to the Center for Computational Mass Spectrometry, MassIVE and the ProteomeXchange Consortium and can be downloaded using the following link ftp://massive.ucsd.edu/MSV000083750 (MassIVE ID number: MSV000083750, ProteomeXchange ID number: PXD013721). Data uploads include the protein identification and quantification details, spectral library and FASTA file used for mass spectrometric analysis. SASP proteomic profiles are available on Panorama (https://panoramaweb.org/project/Schilling/SASP_Atlas_Buck/begin.view?), a repository for targeted mass spectrometry assays generated in Skyline software [52,53]. All data are available for viewing and downloading on SASP Atlas (www.saspatlas.com).

MassIVE: MSV000083750 **(**ftp://massive.ucsd.edu/MSV000083750)

ProteomeXchange: PXD013721 (http://proteomecentral.proteomexchange.org/cgi/GetDataset?ID=PXD013721)

SASP Atlas: www.SASPAtlas.com

SASP Panels: https://panoramaweb.org/project/Schilling/SASP_Atlas_Buck/begin.view?

Acknowledgments: We thank John C.W. Carroll for graphical support generating figures.

Funding: This work was supported by grants from the National Institute on Aging (U01 AG060906-01, PI: Schilling; P01AG017242 and R01AG051729, PI: Campisi) and a

National Institutes of Health Shared Instrumentation Grant (1S10 OD016281, Buck Institute). N.B. and O.J. were supported by postdoctoral fellowships from the Glenn Foundation for Medical Research. A.K. was supported by the SENS Foundation. V.S. was supported by the University of Washington, Seattle Proteomics Resource (UWPR95794).

Competing interests: J.C. is a founder and share holder of Unity Biotechnology, which develops senolytic drugs. The other authors have declared no competing interests.

Author Contributions: Conceptualization, N.B., B.S., J.C. L.F.; Cell Culture, N.B., A.K., O.J., C.K., T.P.; RNA expression and Activity Assays, N.B., A.K., O.J., C.K. T.P.; Proteomic Sample Preparation, N.B., T.P., A.H., S.S.; Data Analysis, N.B., B.S., A.H., S.S.; Pathway and Network Analysis, N.B., C.R.; Visualization, N.B., C.R.; Web Database, V.S., C.R., N.B, B.S.; Writing and Editing, N.B., B.S., J.C., L.F.; Funding Acquisition, B.S., J.C.

References

1. Acosta JC, O'Loghlen A, Banito A, Guijarro MV, Augert A, Raguz S, et al. Chemokine signaling via the CXCR2 receptor reinforces senescence. Cell. 2008;133: 1006–1018. doi:10.1016/j.cell.2008.03.038

2. Coppé J-P, Patil CK, Rodier F, Sun Y, Muñoz DP, Goldstein J, et al. Senescence-Associated Secretory Phenotypes Reveal Cell-Nonautonomous Functions of Oncogenic RAS and the p53 Tumor Suppressor. PLOS Biology. 2008;6: e301. doi:10.1371/journal.pbio.0060301

3. Coppé J-P, Patil CK, Rodier F, Krtolica A, Beauséjour CM, Parrinello S, et al. A Human-Like Senescence-Associated Secretory Phenotype Is Conserved in Mouse Cells Dependent on Physiological Oxygen. PLoS One. 2010;5: e9188. doi:10.1371/journal.pone.0009188

4. Kuilman T, Michaloglou C, Vredeveld LCW, Douma S, van Doorn R, Desmet CJ, et al. Oncogene-induced senescence relayed by an interleukin-dependent inflammatory network. Cell. 2008;133: 1019–1031. doi:10.1016/j.cell.2008.03.039

5. Neves J, Demaria M, Campisi J, Jasper H. Of flies, mice, and men: evolutionarily conserved tissue damage responses and aging. Dev Cell. 2015;32: 9–18. doi:10.1016/j.devcel.2014.11.028

6. Tchkonia T, Zhu Y, van Deursen J, Campisi J, Kirkland JL. Cellular senescence and the senescent secretory phenotype: therapeutic opportunities. J Clin Invest. 2013;123: 966–72. doi:10.1172/JCI64098

676 7. Tominaga K. The emerging role of senescent cells in tissue homeostasis and
677 pathophysiology. Pathobiol Aging Age Relat Dis. 2015;5.
678 doi:10.3402/pba.v5.27743

679 8. Baker DJ, Wijshake T, Tchkonia T, LeBrasseur NK, Childs BG, van de Sluis B, et
680 al. Clearance of p16^{Ink4a}-positive senescent cells delays ageing-associated
681 disorders. Nature. 2011;479: 232–236. doi:10.1038/nature10600

682 9. Demaria M, Ohtani N, Youssef SA, Rodier F, Toussaint W, Mitchell JR, et al. An
683 Essential Role for Senescent Cells in Optimal Wound Healing through Secretion of
684 PDGF-AA. Dev Cell. 2014;31: 722–733. doi:10.1016/j.devcel.2014.11.012

685 10. Childs BG, Baker DJ, Wijshake T, Conover CA, Campisi J, van Deursen JM.
686 Senescent intimal foam cells are deleterious at all stages of atherosclerosis.
687 Science. 2016;354: 472–477. doi:10.1126/science.aaf6659

688 11. Jeon OH, David N, Campisi J, Elisseeff JH. Senescent cells and osteoarthritis: a
689 painful connection. J Clin Invest. 2018;128: 1229–1237. doi:10.1172/JCI95147

690 12. Baar MP, Brandt RMC, Putavet DA, Klein JDD, Derks KWJ, Bourgeois BRM, et al.
691 Targeted Apoptosis of Senescent Cells Restores Tissue Homeostasis in Response
692 to Chemotoxicity and Aging. Cell. 2017;169: 132-147.e16.
693 doi:10.1016/j.cell.2017.02.031

694 13. Demaria M, O'Leary MN, Chang J, Shao L, Liu S, Alimirah F, et al. Cellular
695 Senescence Promotes Adverse Effects of Chemotherapy and Cancer Relapse.
696 Cancer Discov. 2017;7: 165–176. doi:10.1158/2159-8290.CD-16-0241

14. Abdul-Aziz AM, Sun Y, Hellmich C, Marlein CR, Mistry J, Forde E, et al. Acute myeloid leukemia induces pro-tumoral p16INK4a driven senescence in the bone marrow microenvironment. Blood. 2018;133: 446–456. doi:10.1182/blood-2018-04-845420

15. Chang J, Wang Y, Shao L, Laberge RM, Demaria M, Campisi J, et al. Clearance of senescent cells by ABT263 rejuvenates aged hematopoietic stem cells in mice. Nat Med. 2016;22: 78–83. doi:10.1038/nm.4010

16. Valentijn FA, Falke LL, Nguyen TQ, Goldschmeding R. Cellular senescence in the aging and diseased kidney. J Cell Commun Signal. 2018;12: 69–82. doi:10.1007/s12079-017-0434-2

17. Baker DJ, Childs BG, Durik M, Wijers ME, Sieben CJ, Zhong J, et al. Naturally occurring p16(Ink4a)-positive cells shorten healthy lifespan. Nature. 2016;530: 184–9. doi:10.1038/nature16932

18. Wiley C, Liu S, Limbad C, Zawadzka A, Beck J, Demaria M, et al. SILAC analysis reveals increased secretion of hemostasis-related factors by senescent cells. Cell Reports. 2019;Forthcoming. Available: https://papers.ssrn.com/abstract=3155773

19. Hernandez-Vallejo SJ, Beaupere C, Larghero J, Capeau J, Lagathu C. HIV protease inhibitors induce senescence and alter osteoblastic potential of human bone marrow mesenchymal stem cells: beneficial effect of pravastatin. Aging Cell. 2013;12: 955–965. doi:10.1111/acel.12119

20. Sedelnikova OA, Redon CE, Dickey JS, Nakamura AJ, Georgakilas AG, Bonner WM. Role of oxidatively induced DNA lesions in human pathogenesis. Mutat Res. 2010;704: 152–159. doi:10.1016/j.mrrev.2009.12.005

21. Di Micco R, Fumagalli M, Cicalese A, Piccinin S, Gasparini P, Luise C, et al. Oncogene-induced senescence is a DNA damage response triggered by DNA hyper-replication. Nature. 2006;444: 638–642. doi:10.1038/nature05327

22. Rodier F, Coppé JP, Patil CK, Hoeijmakers WA, Muñoz DP, Raza SR, et al. Persistent DNA damage signalling triggers senescence-associated inflammatory cytokine secretion. Nat Cell Biol. 2009;11: 973–9. doi:10.1038/ncb1909

23. Coppé J-P, Desprez P-Y, Krtolica A, Campisi J. The Senescence-Associated Secretory Phenotype: The Dark Side of Tumor Suppression. Annu Rev Pathol. 2010;5: 99–118. doi:10.1146/annurev-pathol-121808-102144

24. Hernandez-Segura A, de Jong TV, Melov S, Guryev V, Campisi J, Demaria M. Unmasking Transcriptional Heterogeneity in Senescent Cells. Curr Biol. 2017;27: 2652-2660.e4. doi:10.1016/j.cub.2017.07.033

25. Özcan S, Alessio N, Acar MB, Mert E, Omerli F, Peluso G, et al. Unbiased analysis of senescence associated secretory phenotype (SASP) to identify common components following different genotoxic stresses. Aging (Albany NY). 2016;8: 1316–1327. doi:10.18632/aging.100971

26. Borghesan M, Fafián-Labora J, Eleftheriadou O, Carpintero-Fernández P, Paez-Ribes M, Vizcay-Barrena G, et al. Small Extracellular Vesicles Are Key Regulators

of Non-cell Autonomous Intercellular Communication in Senescence via the Interferon Protein IFITM3. Cell Reports. 2019;27: 3956-3971.e6. doi:10.1016/j.celrep.2019.05.095

27. Lehmann BD, Paine MS, Brooks AM, McCubrey JA, Renegar RH, Wang R, et al. Senescence-associated exosome release from human prostate cancer cells. Cancer Res. 2008;68: 7864–7871. doi:10.1158/0008-5472.CAN-07-6538

28. Takasugi M. Emerging roles of extracellular vesicles in cellular senescence and aging. Aging Cell. 2018;17. doi:10.1111/acel.12734

29. Jeon OH, Wilson DR, Clement CC, Rathod S, Cherry C, Powell B, et al. Senescence cell-associated extracellular vesicles serve as osteoarthritis disease and therapeutic markers. JCI Insight. 2019;4. doi:10.1172/jci.insight.125019

30. Gillet LC, Navarro P, Tate S, Röst H, Selevsek N, Reiter L, et al. Targeted data extraction of the MS/MS spectra generated by data-independent acquisition: a new concept for consistent and accurate proteome analysis. Mol Cell Proteomics. 2012;11: O111.016717. doi:10.1074/mcp.O111.016717

31. Schilling B, Gibson BW, Hunter CL. Generation of High-Quality SWATH® Acquisition Data for Label-free Quantitative Proteomics Studies Using TripleTOF® Mass Spectrometers. Methods Mol Biol. 2017;1550: 223–233. doi:10.1007/978-1-4939-6747-6_16

32. Bruderer R, Bernhardt OM, Gandhi T, Miladinović SM, Cheng LY, Messner S, et al. Extending the limits of quantitative proteome profiling with data-independent

759 acquisition and application to acetaminophen-treated three-dimensional liver
760 microtissues. Mol Cell Proteomics. 2015;14: 1400–10.
761 doi:10.1074/mcp.M114.044305

762 33. Bindea G, Mlecnik B, Hackl H, Charoentong P, Tosolini M, Kirilovsky A, et al.
763 ClueGO: a Cytoscape plug-in to decipher functionally grouped gene ontology and
764 pathway annotation networks. Bioinformatics. 2009;25: 1091–1093.
765 doi:10.1093/bioinformatics/btp101

766 34. Shannon P, Markiel A, Ozier O, Baliga NS, Wang JT, Ramage D, et al. Cytoscape:
767 a software environment for integrated models of biomolecular interaction networks.
768 Genome Res. 2003;13: 2498–2504. doi:10.1101/gr.1239303

769 35. Kaur G, Levy E. Cystatin C in Alzheimer's disease. Front Mol Neurosci. 2012;5.
770 doi:10.3389/fnmol.2012.00079

771 36. O'Brien RJ, Wong PC. Amyloid Precursor Protein Processing and Alzheimer's
772 Disease. Annu Rev Neurosci. 2011;34: 185–204. doi:10.1146/annurev-neuro-
773 061010-113613

774 37. Bonifati V, Rizzu P, van Baren MJ, Schaap O, Breedveld GJ, Krieger E, et al.
775 Mutations in the DJ-1 gene associated with autosomal recessive early-onset
776 parkinsonism. Science. 2003;299: 256–259. doi:10.1126/science.1077209

777 38. Chang AC-M, Doherty J, Huschtscha LI, Redvers R, Restall C, Reddel RR, et al.
778 STC1 expression is associated with tumor growth and metastasis in breast cancer.
779 Clin Exp Metastasis. 2015;32: 15–27. doi:10.1007/s10585-014-9687-9

780 39. Du Y-Z, Gu X-H, Cheng S-F, Li L, Liu H, Hu L-P, et al. The oncogenetic role of
781 stanniocalcin 1 in lung adenocarcinoma: a promising serum candidate biomarker
782 for tracking lung adenocarcinoma progression. Tumour Biol. 2016;37: 5633–5644.
783 doi:10.1007/s13277-015-4431-x

784 40. Ohkouchi S, Ono M, Kobayashi M, Hirano T, Tojo Y, Hisata S, et al. Myriad
785 Functions of Stanniocalcin-1 (STC1) Cover Multiple Therapeutic Targets in the
786 Complicated Pathogenesis of Idiopathic Pulmonary Fibrosis (IPF). Clin Med
787 Insights Circ Respir Pulm Med. 2015;9: 91–96. doi:10.4137/CCRPM.S23285

788 41. Pan JS-C, Huang L, Belousova T, Lu L, Yang Y, Reddel R, et al. Stanniocalcin-1
789 Inhibits Renal Ischemia/Reperfusion Injury via an AMP-Activated Protein Kinase-
790 Dependent Pathway. J Am Soc Nephrol. 2015;26: 364–378.
791 doi:10.1681/ASN.2013070703

792 42. Shahim P, Blennow K, Johansson P, Svensson J, Lista S, Hampel H, et al.
793 Cerebrospinal Fluid Stanniocalcin-1 as a Biomarker for Alzheimer's Disease and
794 Other Neurodegenerative Disorders. Neuromolecular Med. 2017;19: 154–160.
795 doi:10.1007/s12017-016-8439-1

796 43. Su J, Guo B, Zhang T, Wang K, Li X, Liang G. Stanniocalcin-1, a new biomarker of
797 glioma progression, is associated with prognosis of patients. Tumour Biol. 2015;36:
798 6333–6339. doi:10.1007/s13277-015-3319-0

799 44. Davalos AR, Kawahara M, Malhotra GK, Schaum N, Huang J, Ved U, et al. p53-
800 dependent release of Alarmin HMGB1 is a central mediator of senescent
801 phenotypes. J Cell Biol. 2013;201: 613–629. doi:10.1083/jcb.201206006

802 45. Keerthikumar S, Chisanga D, Ariyaratne D, Al Saffar H, Anand S, Zhao K, et al.
803 ExoCarta: A Web-Based Compendium of Exosomal Cargo. Journal of Molecular
804 Biology. 2016;428: 688–692. doi:10.1016/j.jmb.2015.09.019

805 46. Belov L, Matic KJ, Hallal S, Best OG, Mulligan SP, Christopherson RI. Extensive
806 surface protein profiles of extracellular vesicles from cancer cells may provide
807 diagnostic signatures from blood samples. J Extracell Vesicles. 2016;5.
808 doi:10.3402/jev.v5.25355

809 47. Tanaka T, Biancotto A, Moaddel R, Moore AZ, Gonzalez-Freire M, Aon MA, et al.
810 Plasma proteomic signature of age in healthy humans. Aging Cell. 2018;17:
811 e12799. doi:10.1111/acel.12799

812 48. Acosta JC, Banito A, Wuestefeld T, Georgilis A, Janich P, Morton JP, et al. A
813 complex secretory program orchestrated by the inflammasome controls paracrine
814 senescence. Nat Cell Biol. 2013;15: 978–90. doi:10.1038/ncb2784

815 49. Nelson G, Wordsworth J, Wang C, Jurk D, Lawless C, Martin-Ruiz C, et al. A
816 senescent cell bystander effect: senescence-induced senescence. Aging Cell.
817 2012;11: 345–349. doi:10.1111/j.1474-9726.2012.00795.x

818 50. Egertson JD, MacLean B, Johnson R, Xuan Y, MacCoss MJ. Multiplexed peptide
819 analysis using data-independent acquisition and Skyline. Nature Protocols.
820 2015;10: 887.

821 51. Rardin MJ, Schilling B, Cheng LY, MacLean BX, Sorensen DJ, Sahu AK, et al.
822 MS1 Peptide Ion Intensity Chromatograms in MS2 (SWATH) Data Independent
823 Acquisitions. Improving Post Acquisition Analysis of Proteomic Experiments. Mol
824 Cell Proteomics. 2015;14: 2405–19. doi:10.1074/mcp.O115.048181

825 52. Sharma V, Eckels J, Taylor GK, Shulman NJ, Stergachis AB, Joyner SA, et al.
826 Panorama: A Targeted Proteomics Knowledge Base. J Proteome Res. 2014;13:
827 4205–4210. doi:10.1021/pr5006636

828 53. Sharma V, Eckels J, Schilling B, Ludwig C, Jaffe JD, MacCoss MJ, et al. Panorama
829 Public: A Public Repository for Quantitative Data Sets Processed in Skyline. Mol
830 Cell Proteomics. 2018;17: 1239–1244. doi:10.1074/mcp.RA117.000543

831 54. Feldman N, Rotter-Maskowitz A, Okun E. DAMPs as mediators of sterile
832 inflammation in aging-related pathologies. Ageing Res Rev. 2015;24: 29–39.
833 doi:10.1016/j.arr.2015.01.003

834 55. Huang J, Xie Y, Sun X, Zeh HJ, Kang R, Lotze MT, et al. DAMPs, Ageing, and
835 Cancer: The 'DAMP Hypothesis.' Ageing Res Rev. 2015;24: 3–16.
836 doi:10.1016/j.arr.2014.10.004

837 56. Franceschi C, Campisi J. Chronic inflammation (inflammaging) and its potential
838 contribution to age-associated diseases. J Gerontol A Biol Sci Med Sci. 2014;69
839 Suppl 1: S4-9. doi:10.1093/gerona/glu057

840 57. Fucikova J, Moserova I, Urbanova L, Bezu L, Kepp O, Cremer I, et al. Prognostic
841 and Predictive Value of DAMPs and DAMP-Associated Processes in Cancer. Front
842 Immunol. 2015;6. doi:10.3389/fimmu.2015.00402

843 58. Garg AD, Galluzzi L, Apetoh L, Baert T, Birge RB, Bravo-San Pedro JM, et al.
844 Molecular and Translational Classifications of DAMPs in Immunogenic Cell Death.
845 Front Immunol. 2015;6. doi:10.3389/fimmu.2015.00588

846 59. Bidadkosh A, Lambooy SPH, Heerspink HJ, Pena MJ, Henning RH, Buikema H, et
847 al. Predictive Properties of Biomarkers GDF-15, NTproBNP, and hs-TnT for
848 Morbidity and Mortality in Patients With Type 2 Diabetes With Nephropathy.
849 Diabetes Care. 2017;40: 784–792. doi:10.2337/dc16-2175

850 60. Daniels LB, Clopton P, Laughlin GA, Maisel AS, Barrett-Connor E. Growth-
851 differentiation factor-15 is a robust, independent predictor of 11-year mortality risk
852 in community-dwelling older adults: the Rancho Bernardo Study. Circulation.
853 2011;123: 2101–2110. doi:10.1161/CIRCULATIONAHA.110.979740

854 61. Ho JE, Mahajan A, Chen M-H, Larson MG, McCabe EL, Ghorbani A, et al. Clinical
855 and genetic correlates of growth differentiation factor 15 in the community. Clin
856 Chem. 2012;58: 1582–1591. doi:10.1373/clinchem.2012.190322

857 62. Ho JE, Hwang S-J, Wollert KC, Larson MG, Cheng S, Kempf T, et al. Biomarkers
858 Of Cardiovascular Stress And Incident Chronic Kidney Disease. Clin Chem.
859 2013;59: 1613–1620. doi:10.1373/clinchem.2013.205716

860 63. Rohatgi A, Patel P, Das SR, Ayers CR, Khera A, Martinez-Rumayor A, et al.
861 Association of growth differentiation factor-15 with coronary atherosclerosis and
862 mortality in a young, multiethnic population: observations from the Dallas Heart
863 Study. Clin Chem. 2012;58: 172–182. doi:10.1373/clinchem.2011.171926

864 64. Wallentin L, Zethelius B, Berglund L, Eggers KM, Lind L, Lindahl B, et al. GDF-15
865 for prognostication of cardiovascular and cancer morbidity and mortality in men.
866 PLoS ONE. 2013;8: e78797. doi:10.1371/journal.pone.0078797

867 65. Wollert KC, Kempf T, Wallentin L. Growth Differentiation Factor 15 as a Biomarker
868 in Cardiovascular Disease. Clinical Chemistry. 2017;63: 140–151.
869 doi:10.1373/clinchem.2016.255174

870 66. Bhat R, Crowe EP, Bitto A, Moh M, Katsetos CD, Garcia FU, et al. Astrocyte
871 senescence as a component of Alzheimer's disease. PLoS ONE. 2012;7: e45069.
872 doi:10.1371/journal.pone.0045069

873 67. Chen Y-K, Tung C-W, Lee J-Y, Hung Y-C, Lee C-H, Chou S-H, et al. Plasma
874 matrix metalloproteinase 1 improves the detection and survival prediction of
875 esophageal squamous cell carcinoma. Scientific Reports. 2016;6: 30057.
876 doi:10.1038/srep30057

877 68. Rosas IO, Richards TJ, Konishi K, Zhang Y, Gibson K, Lokshin AE, et al. MMP1
878 and MMP7 as Potential Peripheral Blood Biomarkers in Idiopathic Pulmonary
879 Fibrosis. PLoS Med. 2008;5. doi:10.1371/journal.pmed.0050093

880 69. Roy R, Yang J, Moses MA. Matrix Metalloproteinases As Novel Biomarkers and
881 Potential Therapeutic Targets in Human Cancer. J Clin Oncol. 2009;27: 5287–
882 5297. doi:10.1200/JCO.2009.23.5556

883 70. Théry C, Amigorena S, Raposo G, Clayton A. Isolation and characterization of
884 exosomes from cell culture supernatants and biological fluids. Curr Protoc Cell Biol.
885 2006;Chapter 3: Unit 3.22. doi:10.1002/0471143030.cb0322s30

886 71. Collins BC, Hunter CL, Liu Y, Schilling B, Rosenberger G, Bader SL, et al. Multi-
887 laboratory assessment of reproducibility, qualitative and quantitative performance
888 of SWATH-mass spectrometry. Nature Communications. 2017;8: 291.
889 doi:10.1038/s41467-017-00249-5

890 72. Rosenberger G, Koh CC, Guo T, Röst HL, Kouvonen P, Collins BC, et al. A
891 repository of assays to quantify 10,000 human proteins by SWATH-MS. Sci Data.
892 2014;1: 140031. doi:10.1038/sdata.2014.31

893 73. Pedregosa F, Varoquaux G, Gramfort A, Michel V, Thirion B, Grisel O, et al. Scikit-
894 learn: Machine Learning in Python. Journal of Machine Learning Research.
895 2011;12: 2825−2830.

74. Warnes GR, Bolker B, Bonebakker L, Gentleman R, Liaw WHA, Lumley T, et al. gplots: Various R Programming Tools for Plotting Data [Internet]. 2019. Available: https://CRAN.R-project.org/package=gplots

75. Chen H. VennDiagram: Generate High-Resolution Venn and Euler Plots [Internet]. 2018. Available: https://CRAN.R-project.org/package=VennDiagram

76. Neuwirth E. RColorBrewer: ColorBrewer Palettes [Internet]. 2014. Available: https://CRAN.R-project.org/package=RColorBrewer

Supporting Information: 5 figures, 5 tables:

Fig S1: Senescence markers induced by IR, RAS and ATV. (A) Representative images of SA-β-Gal staining of senescent and control (quiescent) primary human lung fibroblasts and renal epithelial cells following induction of senescence by either IR, RAS or ATV. (B) Quantification of SA-β-Gal positive cells. (C) Levels of $p16^{INK4a}$ and Il-6 mRNAs determined by qPCR and expressed as fold change of senescent over control (red line) cells. (D) Commonly reported SASP factors for each inducer, cell type and fraction. IR = X-irradiation, RAS = RAS oncogene overexpression, ATV = atazanavir treatment, Fib = fibroblasts, Epi = renal epithelial cells.

Fig S2: **Cell viability assays. (**A) Amount of cell death over a 24-hour period as determined by Sytox Green viability dye assay. (B) Fraction of viable cells measured by exclusion of propidium iodide fluorescence, assessed by flow cytometry.

Fig S3: Western Blot Confirmation of top core SASP factors. (A) Western blot exposures of top core SASP factors, GDF15, STC1, SERPINE1, and MMP1, in non-senescent control fibroblasts, early senescent fibroblasts (4 days RAS induction), and fully senescent fibroblasts (7 days RAS induction). (B) Densitometry analysis of western blot. *P-value < 0.05 versus CTL.

Fig S4: Exosome/EV proteomic markers and size distribution analysis. (A) Table of exosome and EV-specific markers identified in exosome and soluble fractions of fibroblasts by mass spectrometry. Multiple peptides from defining exosome/EV markers

were identified in the exosome fractions of RAS and IR-induced senescence experiments but none were detected in the soluble fractions. (B) Table showing EVs secreted per cell and average EV diameter in senescent and control cells in complete (10% FBS) medium and low-serum (0.2% FBS) medium. (C) Size distribution analysis of EVs secreted by senescent and control cells in complete and low-serum medium. (D) Exosome/EV-specific markers detected in isolated EV fractions in each treatment group, as measured by MACSPlex exosome detection kit. (E) Median levels of every surface marker measured in exosome/EV fractions by MACSPlex exosome detection kit. IR = X-irradiation, RAS = RAS oncogene overexpression, FBS = fetal bovine serum.

Fig S5: **Comparison of proteomic and transcriptomic changes in the fibroblast SASP.** Transcriptomic changes in the SASP of fibroblasts reported in a recent meta-analysis (23) (Hernandez-Segura et al., 2017) was compared with proteomic changes in the SASP of the current study. (A) Comparison of transcriptomic meta-analysis and proteomic analysis of secretomes in IR-induced senescent cells compared with non-senescent cells. (B) Venn diagram comparing RAS-induced senescence changes at the transcriptome and secreted proteome level. (C) Venn diagram of the core senescent transcriptome signature (genes changed at senescence regardless of inducer) versus changes common to IR and RAS induced senescence at the secreted proteome level. (D) Venn diagram comparing the senescent transcriptome and secreted proteome core signatures. IR = x-irradiation, RAS = RAS oncogene overexpression.

Table S1: Mass spectrometry quantification for each dataset as separate worksheets in a single excel workbook.

Table S2: Proteins with significantly increased secretion in response to all senescence-inducers.

Table S3: Proteins with significantly increased secretion in all cell types in response to all senescence inducers.

Table S4: Age-associated plasma proteins also present in the SASP as determined in our proteomics experiments.

Table S5: Reagents and Resources.

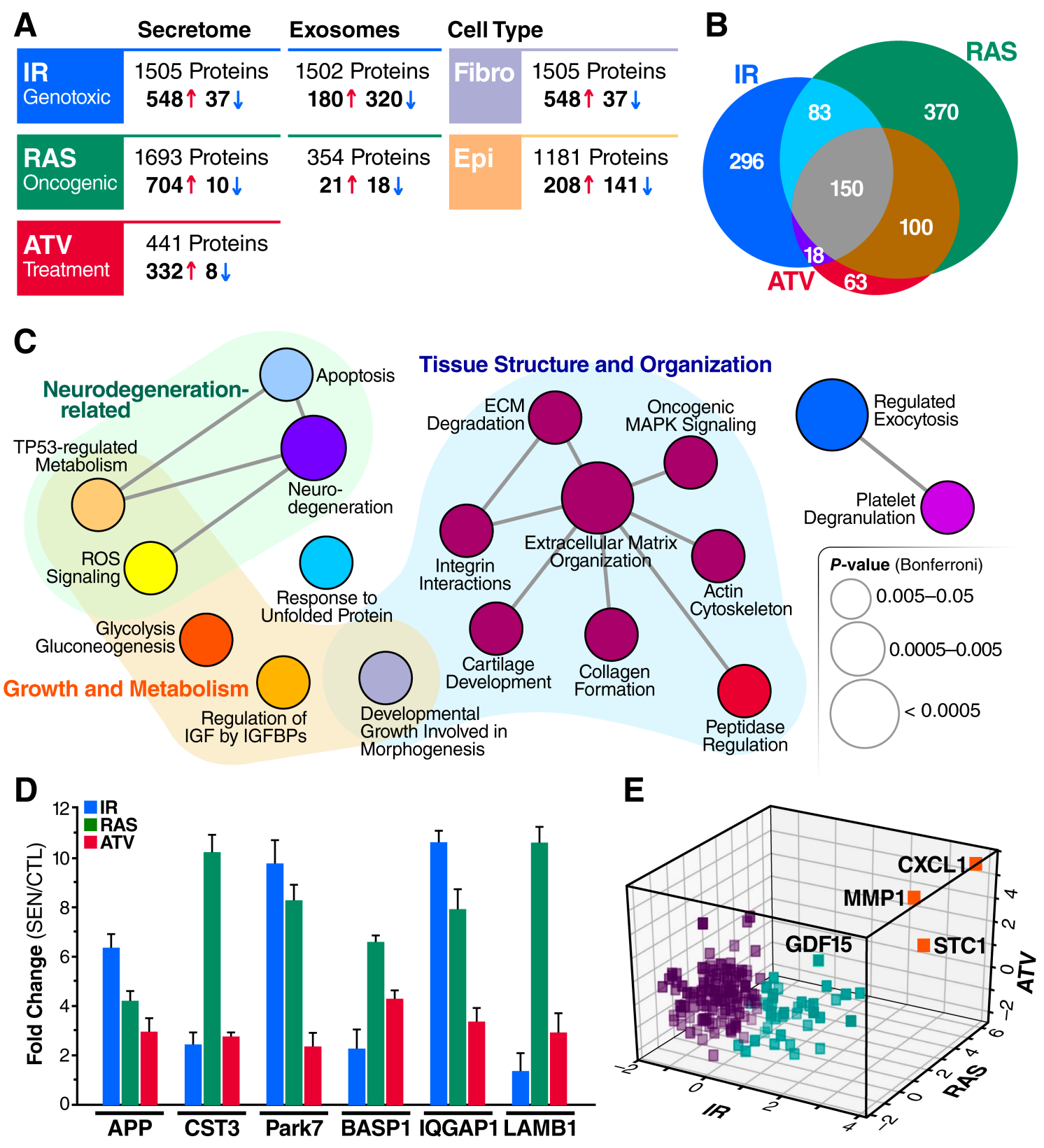
A
Secretome
Exosomes
Cell Type
IR
Genotoxic
1505 Proteins
548↑ 37↓
1502 Proteins
180↑ 320↓
Fibro
1505 Proteins
548↑ 37↓
RAS
Oncogenic
1693 Proteins
704↑ 10↓
354 Proteins
21↑ 18↓
Epi
1181 Proteins
208↑ 141↓
ATV
Treatment
441 Proteins
332↑ 8↓
B
IR
RAS
ATV
296
83
370
150
100
18
63
C
Neurodegeneration-related
Apoptosis
TP53-regulated Metabolism
Neuro-degeneration
ROS Signaling
Response to Unfolded Protein
Glycolysis Gluconeogenesis
Growth and Metabolism
Regulation of IGF by IGFBPs
Developmental Growth Involved in Morphogenesis
Tissue Structure and Organization
ECM Degradation
Oncogenic MAPK Signaling
Integrin Interactions
Extracellular Matrix Organization
Actin Cytoskeleton
Cartilage Development
Collagen Formation
Peptidase Regulation
Regulated Exocytosis
Platelet Degranulation
P-value (Bonferroni)
0.005–0.05
0.0005–0.005
< 0.0005
D
IR
RAS
ATV
Fold Change (SEN/CTL)
0
2
4
6
8
10
12
APP
CST3
Park7
BASP1
IQGAP1
LAMB1
E
CXCL1
MMP1
GDF15
STC1
IR
RAS
ATV

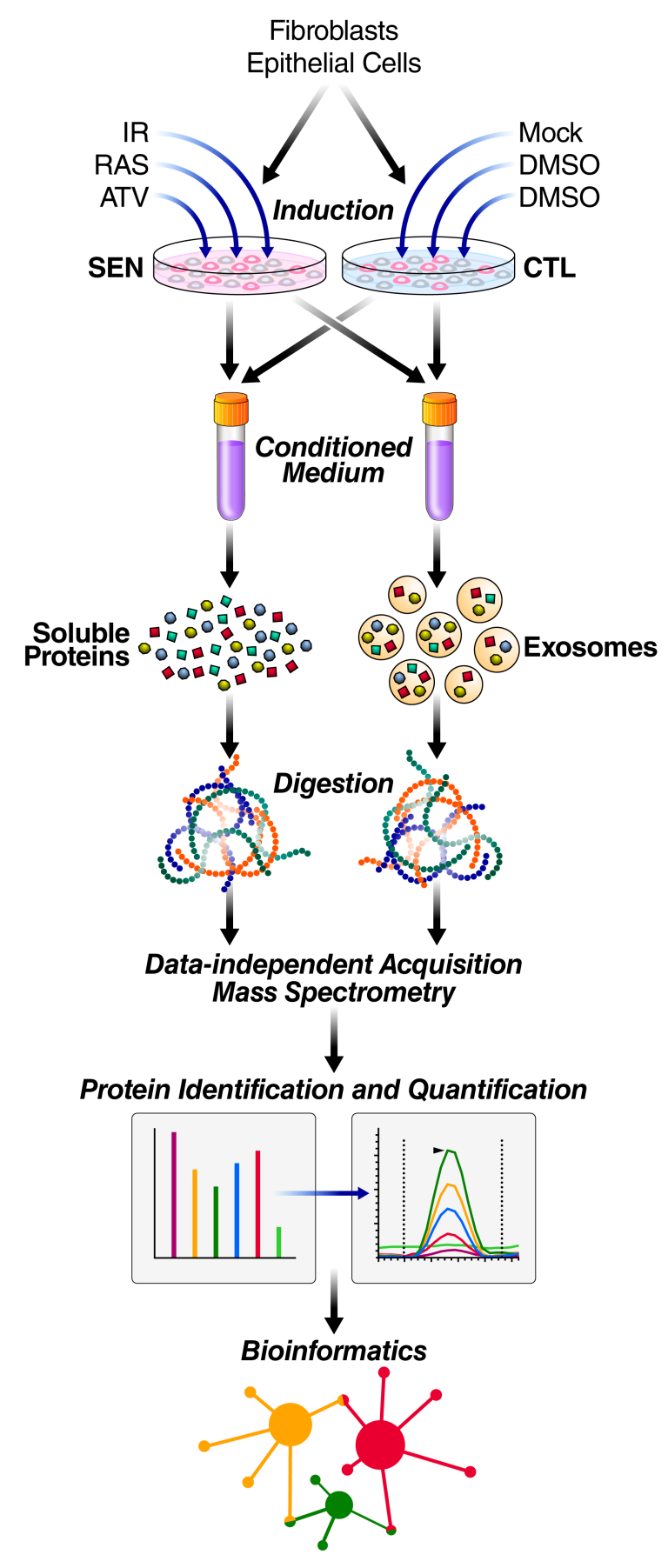
Fibroblasts
Epithelial Cells
IR
RAS
ATV
Induction
Mock
DMSO
DMSO
SEN
CTL
Conditioned Medium
Soluble Proteins
Exosomes
Digestion
Data-independent Acquisition Mass Spectrometry
Protein Identification and Quantification
Bioinformatics

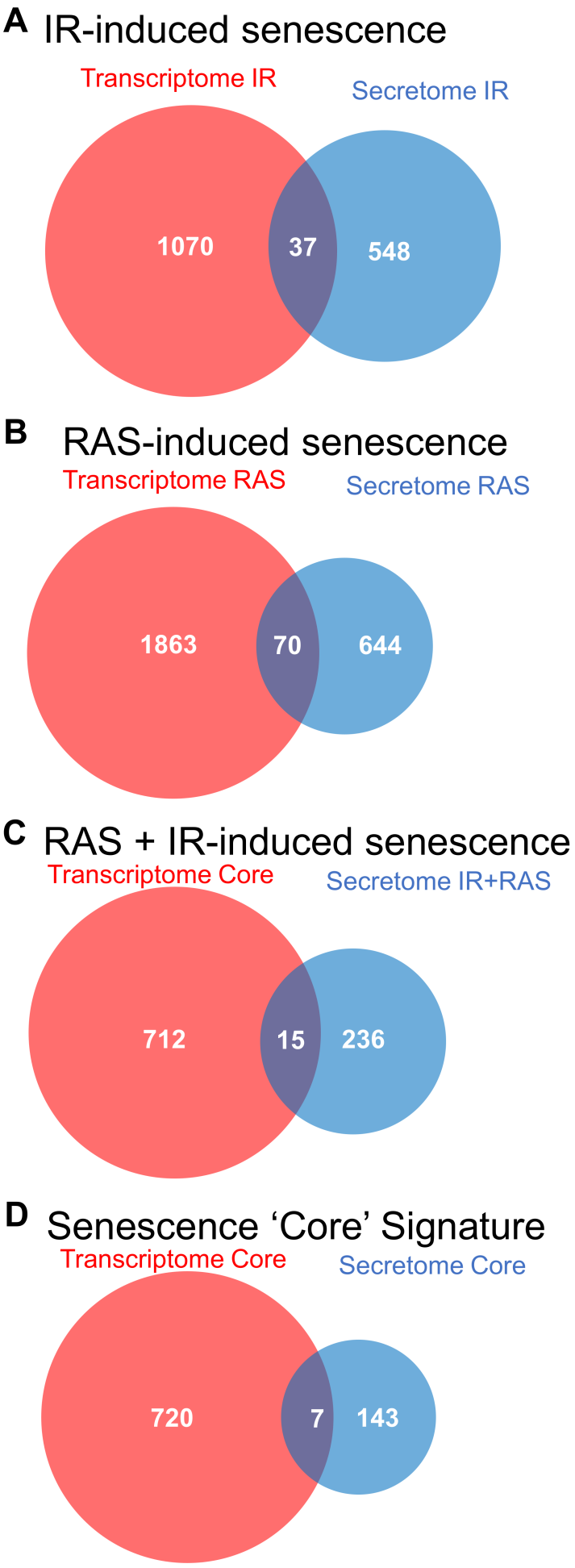
A
IR-induced senescence
Transcriptome IR
Secretome IR
1070
37
548
B
RAS-induced senescence
Transcriptome RAS
Secretome RAS
1863
70
644
C
RAS + IR-induced senescence
Transcriptome Core
Secretome IR+RAS
712
15
236
D
Senescence 'Core' Signature
Transcriptome Core
Secretome Core
720
7
143

D

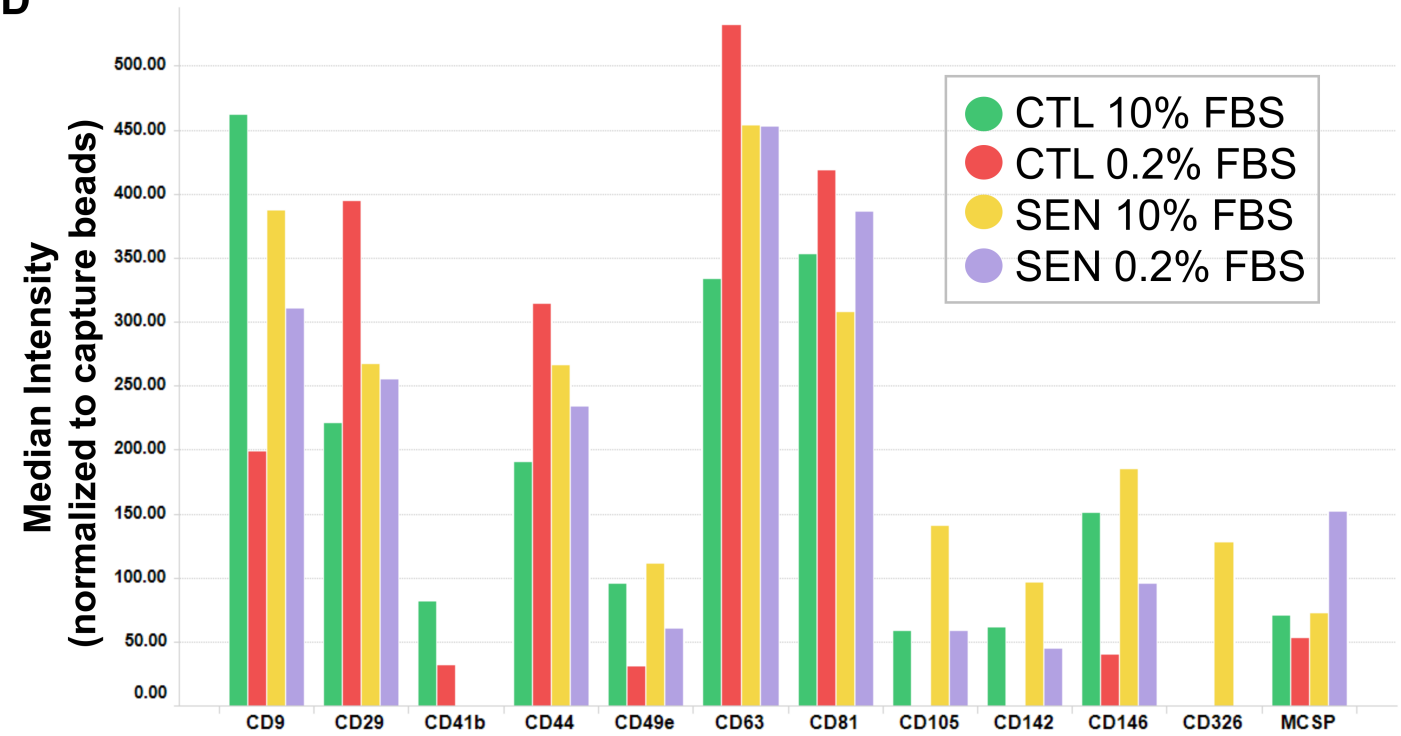
Median Intensity
(normalized to capture beads)
500.00
450.00
400.00
350.00
300.00
250.00
200.00
150.00
100.00
50.00
0.00
CTL 10% FBS
CTL 0.2% FBS
SEN 10% FBS
SEN 0.2% FBS
CD9
CD29
CD41b
CD44
CD49e
CD63
CD81
CD105
CD142
CD146
CD326
MCSP

E

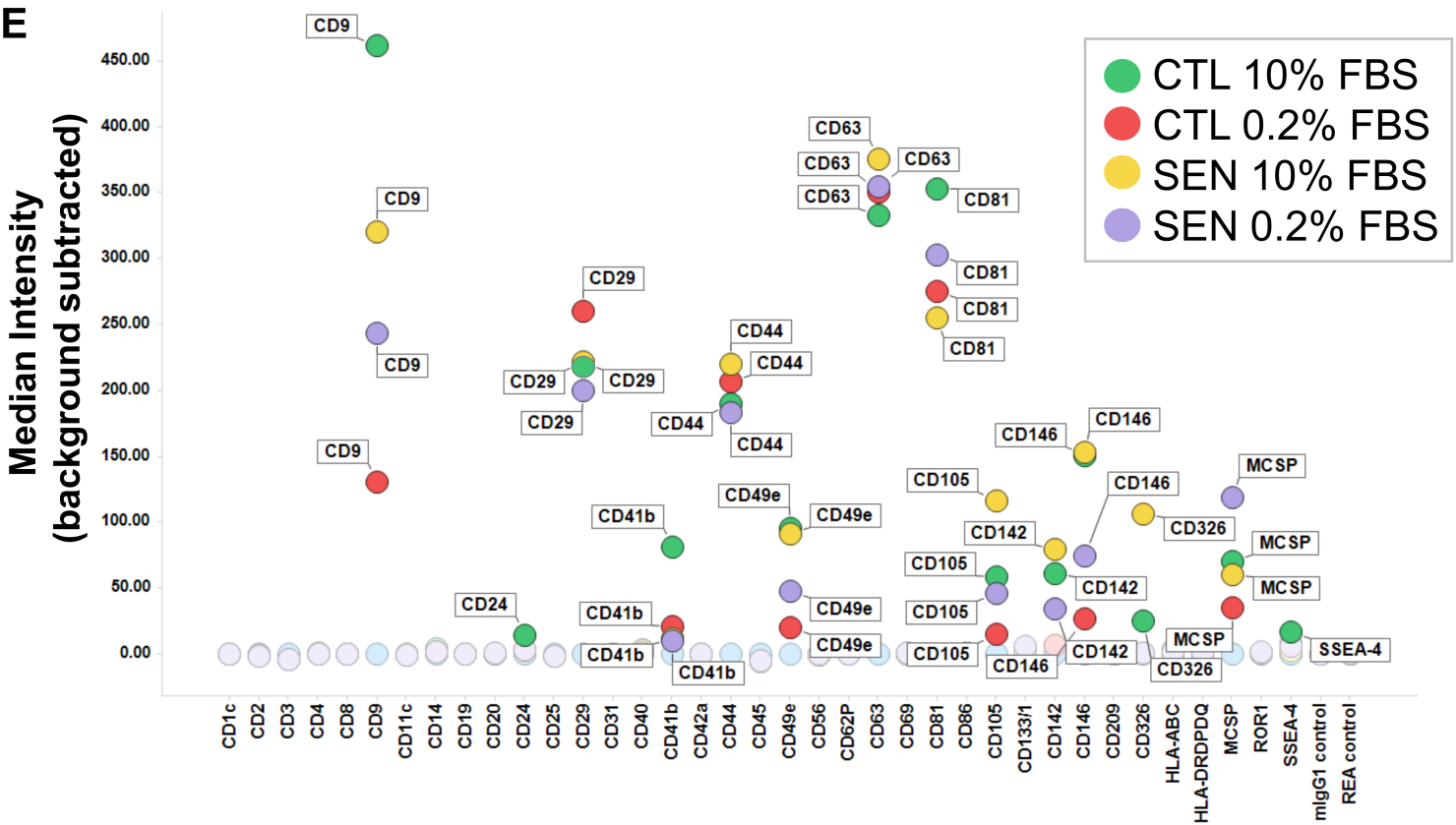
Median Intensity
(background subtracted)
450.00
400.00
350.00
300.00
250.00
200.00
150.00
100.00
50.00
0.00
CTL 10% FBS
CTL 0.2% FBS
SEN 10% FBS
SEN 0.2% FBS
CD1c
CD2
CD3
CD4
CD8
CD9
CD11c
CD14
CD19
CD20
CD24
CD25
CD29
CD31
CD40
CD41b
CD42a
CD44
CD45
CD49e
CD56
CD62P
CD63
CD69
CD81
CD86
CD105
CD133/1
CD142
CD146
CD209
CD326
HLA-ABC
HLA-DRDPDQ
MCSP
ROR1
SSEA-4
mIgG1 control
REA control

A

Number of unique peptides

	Exosome/EV Fraction		Soluble Fraction	
	IR	RAS	IR	RAS
CD63	6	6	0	0
CD9	7	7	0	0
CD81	5	5	0	0
CDC42	20	20	0	0

B

	EVs/Cell	Avg diameter (nm)
CTL 10% FBS	100.88	154
CTL 0.2% FBS	49.90	150
SEN 10% FBS	67.86	147
SEN 0.2% FBS	467.60	143

C

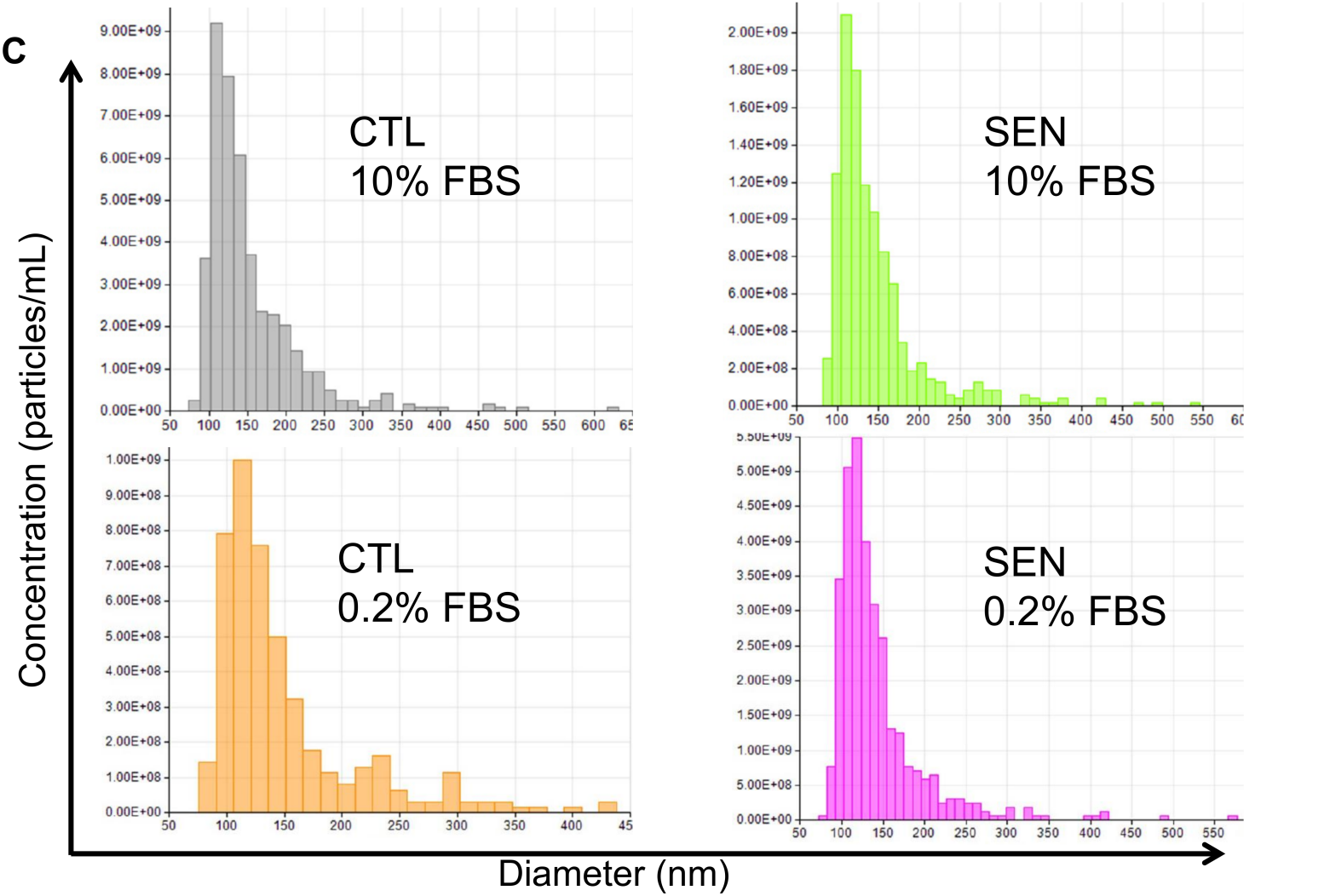

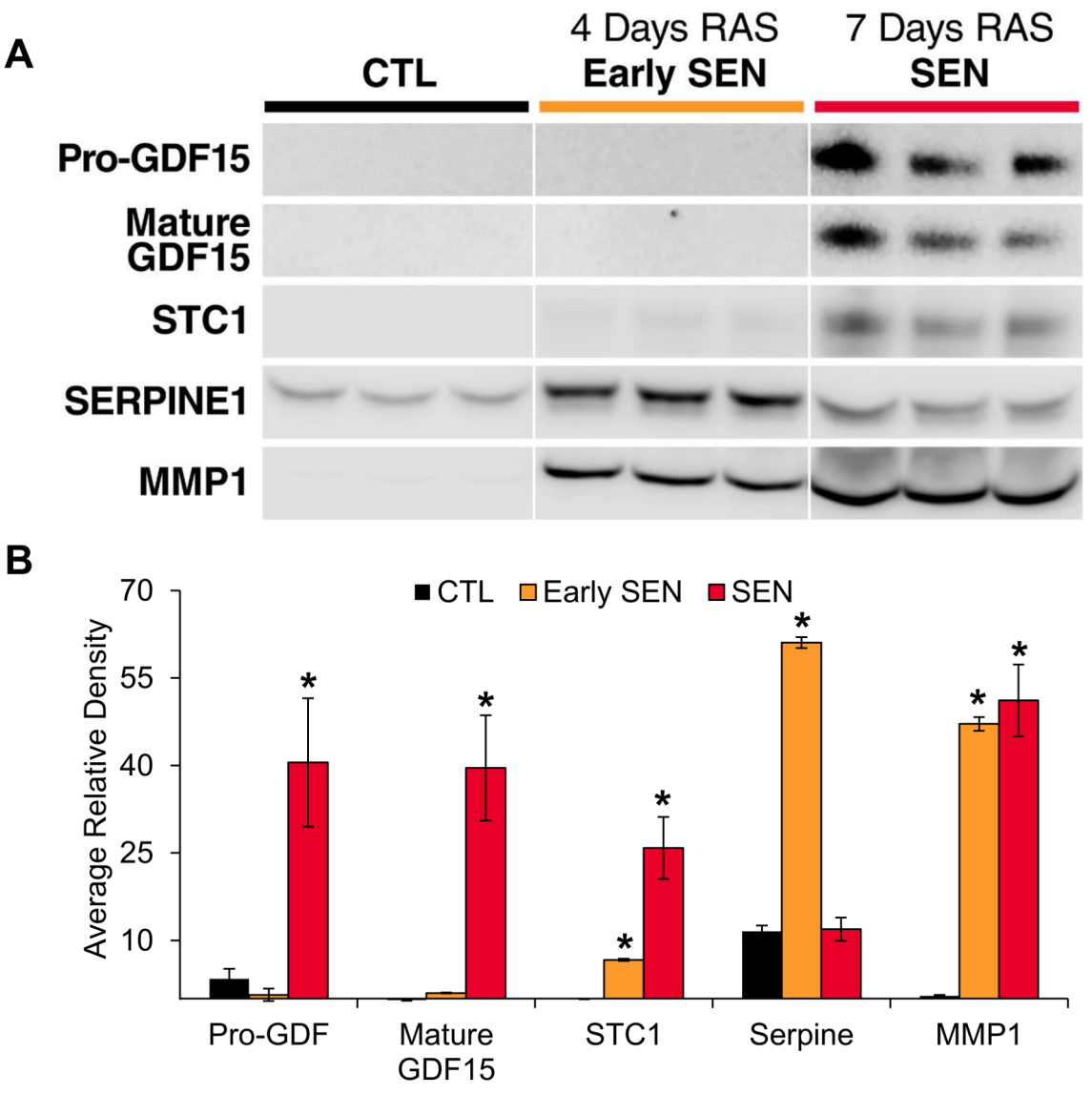
A
CTL
4 Days RAS
Early SEN
7 Days RAS
SEN
Pro-GDF15
Mature
GDF15
STC1
SERPINE1
MMP1
B
CTL
Early SEN
SEN
Average Relative Density
70
55
40
25
10
Pro-GDF
Mature
GDF15
STC1
Serpine
MMP1

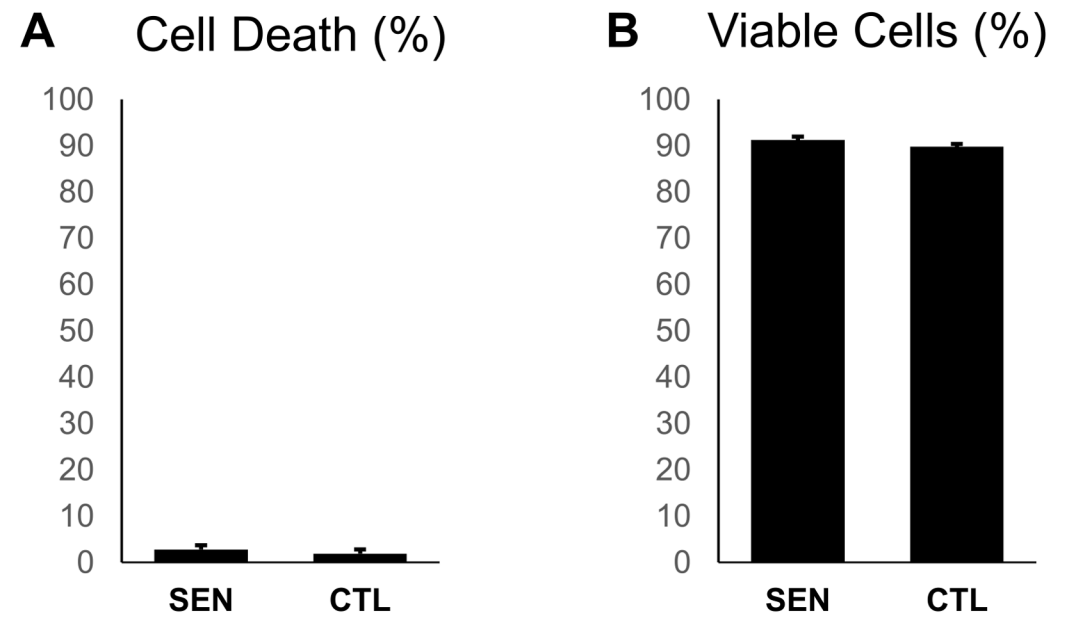
A
Cell Death (%)
100
90
80
70
60
50
40
30
20
10
0
SEN
CTL
B
Viable Cells (%)
100
90
80
70
60
50
40
30
20
10
0
SEN
CTL

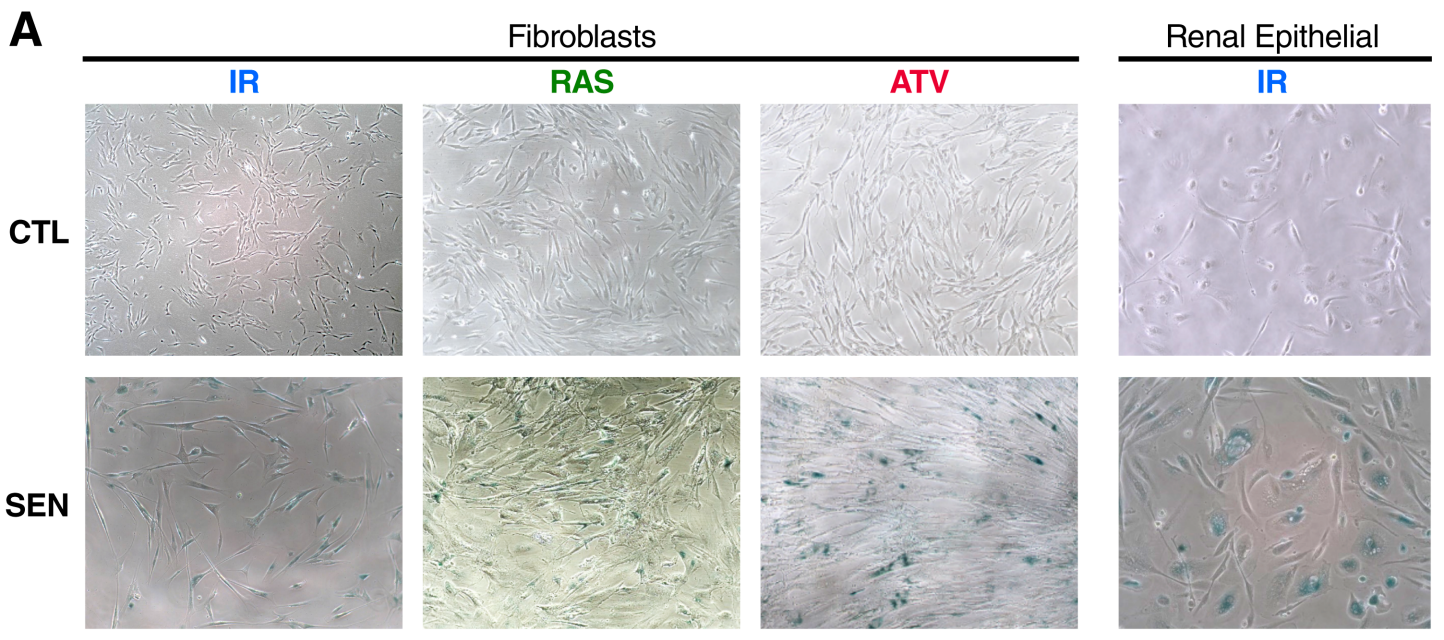

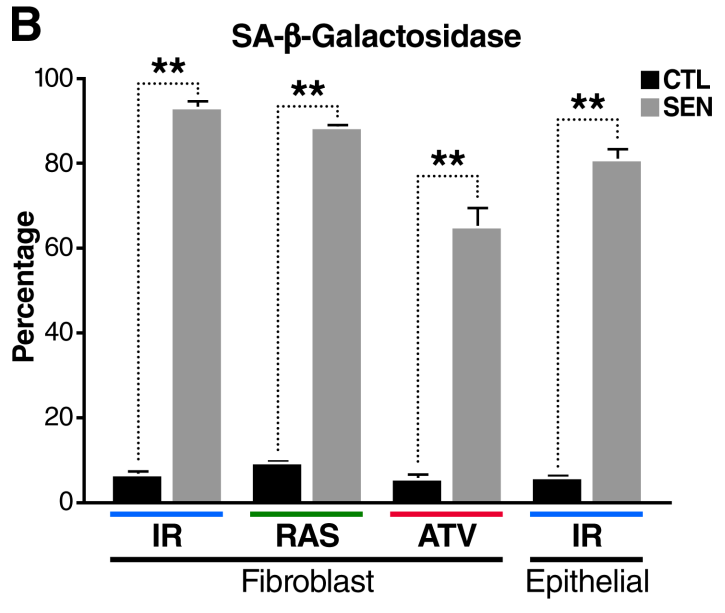

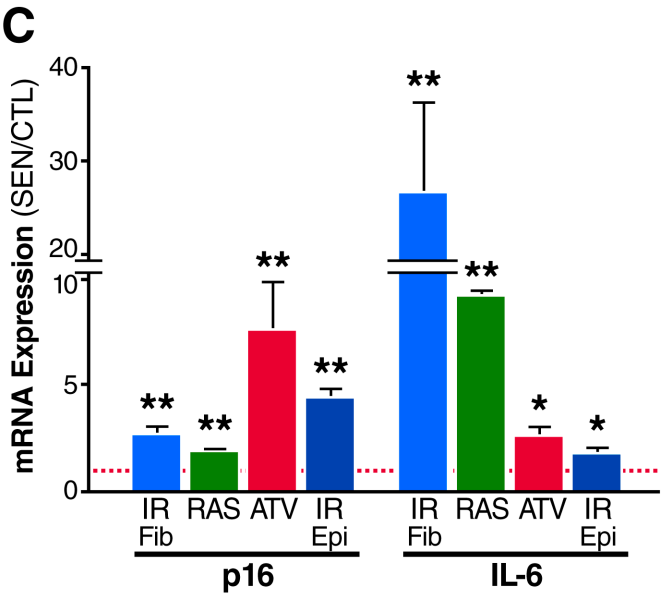

C

		Proteins							RNA		Activity
		CXCL1	CXCL8	HMGB1	IGFBP: 2|3|4|5|7	MMP1 MMP2	LAMB1	TIMP1 TIMP2	p16	IL-6	SA-β-Gal
Fibro	IR	↑	↑	↑	↑↑↑↑↑	↑↑	↑	↑↑	↑	↑	↑
	RAS	↑	↑	↑	↑↑↑↑↑	↑↑	↑	↑↑	↑	↑	↑
	ATV	↑	–	↑	↑↑↑↑↑	↑↑	↑	↑↑	↑	↑	↑
Epi	IR	↓	–	–	↑–↓–↓	––	↓	↓↓	↑	↑	↑
Exo-some	IR	–	–	↑	–↓↓↓↓	–↓	↓	↓↓			
	RAS	–	–	–	––↑––	––	–	–			

SASP Atlas

Genotoxic Stress
Oncogenic Stress
Treatment Stress

Fibroblasts
Epithelial Cells

Soluble Proteins

Exosomes

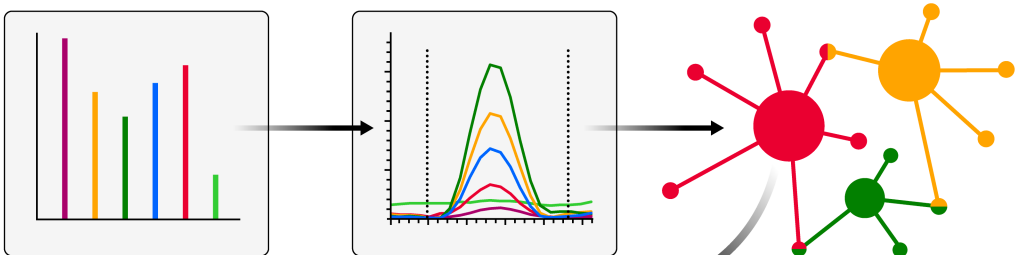

Protein Identification, Quantification, and Bioinformatics

Proteomic Panels | SASP Database

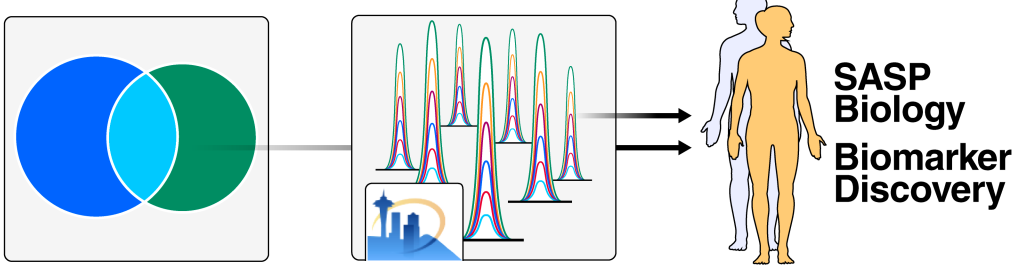

SASP Biology

Biomarker Discovery

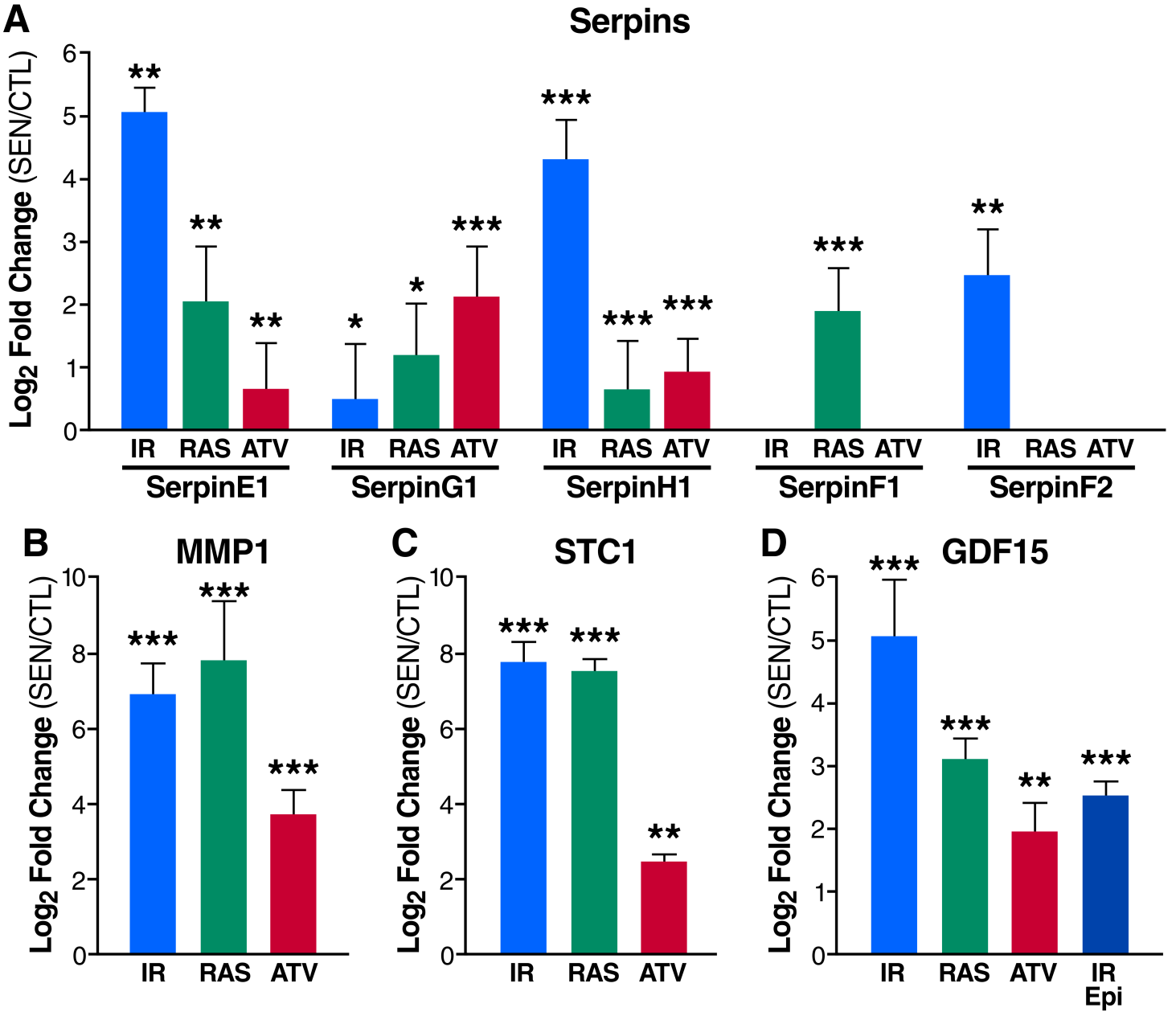
A
Serpins
Log2 Fold Change (SEN/CTL)
IR RAS ATV
SerpinE1
SerpinG1
SerpinH1
SerpinF1
SerpinF2
B
MMP1
C
STC1
D
GDF15
IR RAS ATV IR Epi

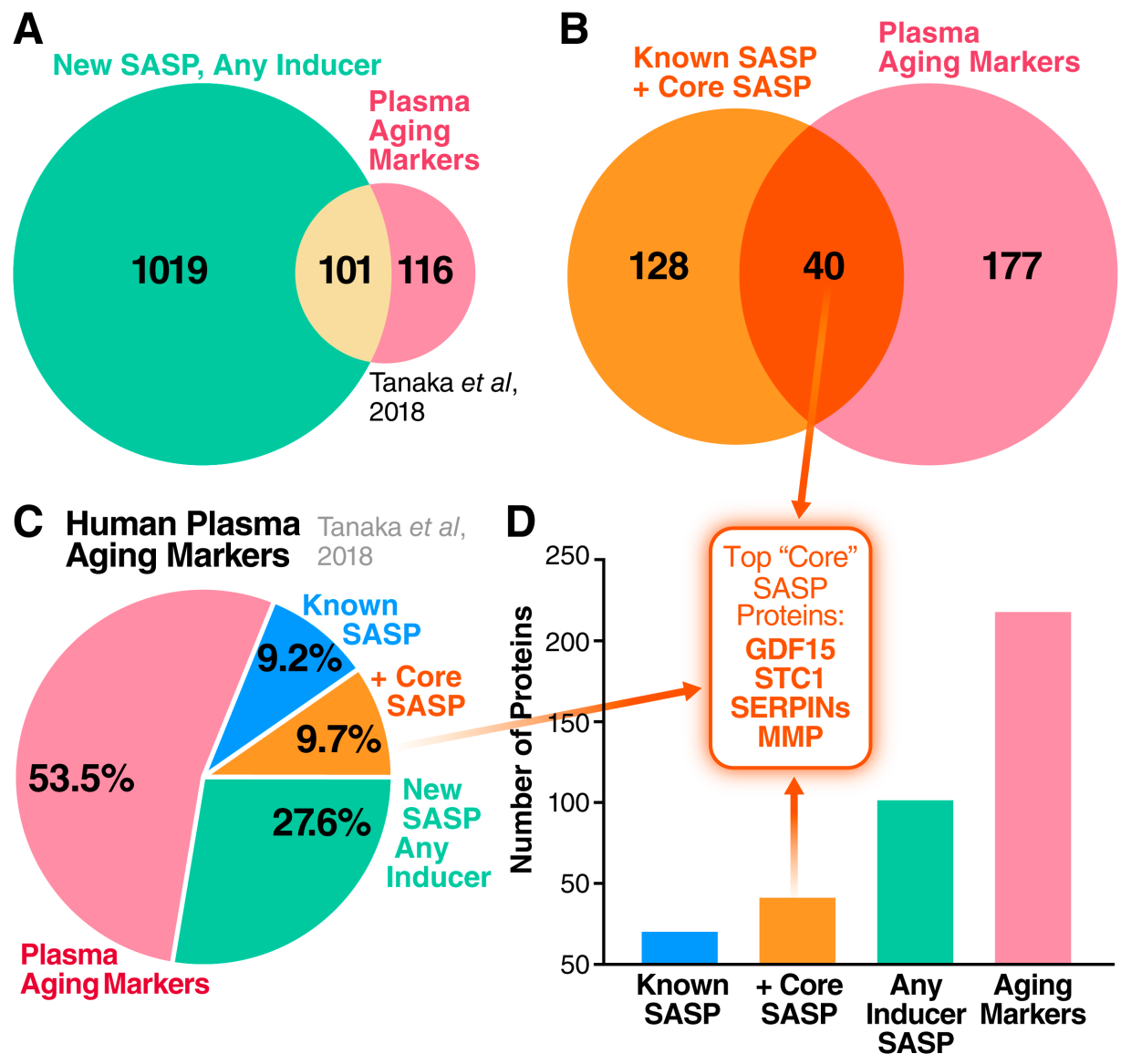
A
New SASP, Any Inducer
Plasma Aging Markers
1019
101
116
Tanaka et al, 2018
B
Known SASP + Core SASP
Plasma Aging Markers
128
40
177
C
Human Plasma Aging Markers
Tanaka et al, 2018
Known SASP
9.2%
+ Core SASP
9.7%
New SASP Any Inducer
27.6%
53.5%
Plasma Aging Markers
D
Top "Core" SASP Proteins:
GDF15
STC1
SERPINs
MMP
Number of Proteins
250
200
150
100
50
50
Known SASP
+ Core SASP
Any Inducer SASP
Aging Markers

A

Genes	IR Log2 SEN/CTL	RAS Log2 SEN/CTL
ANXA1	1.43	6.19
ANXA2	1.82	2.91
ENO3	1.52	1.13
AHNAK	1.21	4.92
SLC1A5	3.71	6.11
ITGA1	–1.52	–1.77
COL6A2	–5.56	–2.32
COL6A1	–5.71	–3.26
COL6A3	–5.65	–6.87

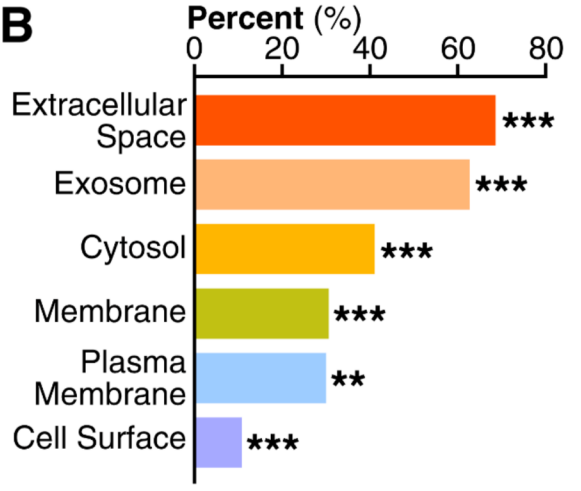

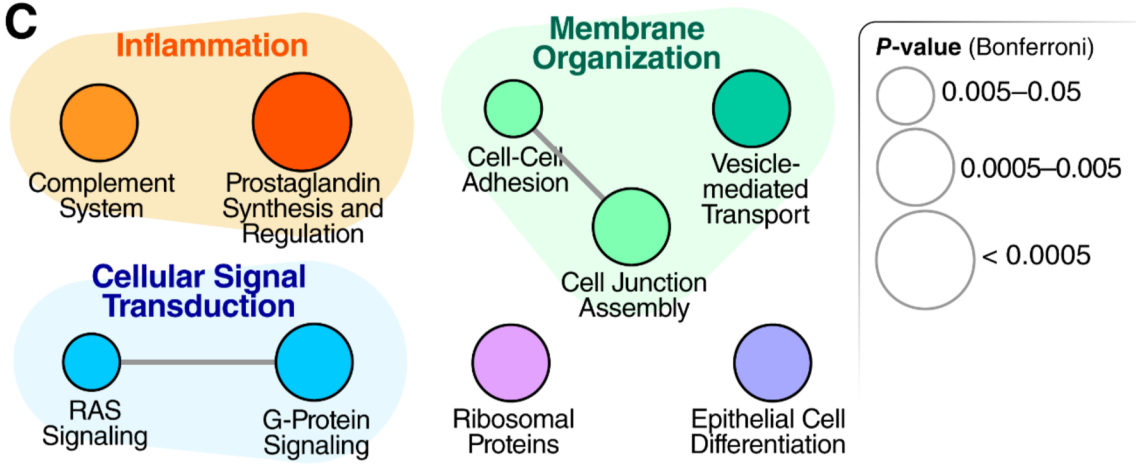

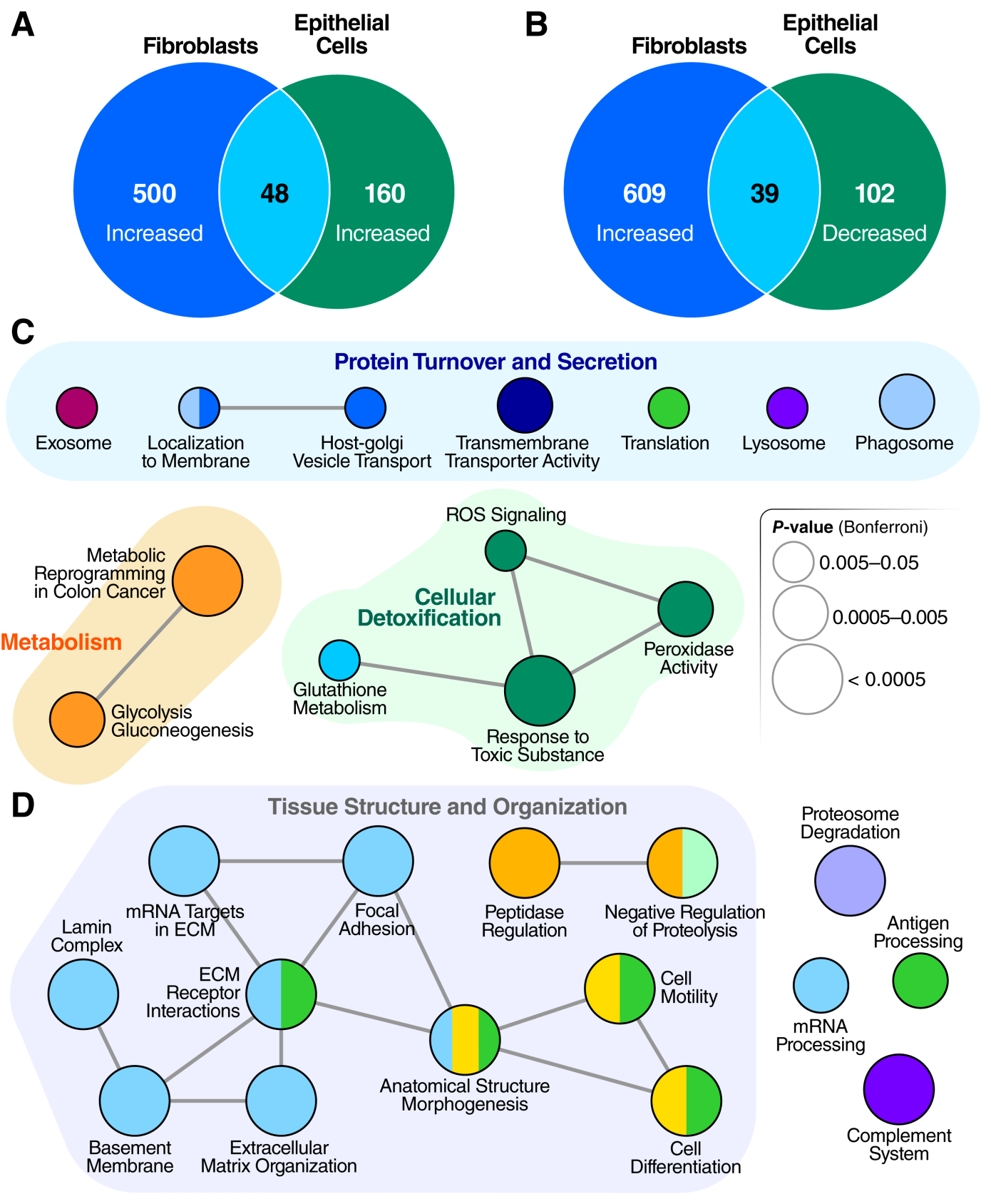
A
Fibroblasts
Epithelial Cells
500
Increased
48
160
Increased
B
Fibroblasts
Epithelial Cells
609
Increased
39
102
Decreased
C
Protein Turnover and Secretion
Exosome
Localization to Membrane
Host-golgi Vesicle Transport
Transmembrane Transporter Activity
Translation
Lysosome
Phagosome
Metabolic Reprogramming in Colon Cancer
Metabolism
Glycolysis Gluconeogenesis
ROS Signaling
Cellular Detoxification
Peroxidase Activity
Glutathione Metabolism
Response to Toxic Substance
P-value (Bonferroni)
0.005–0.05
0.0005–0.005
< 0.0005
D
Tissue Structure and Organization
mRNA Targets in ECM
Focal Adhesion
Peptidase Regulation
Negative Regulation of Proteolysis
Lamin Complex
ECM Receptor Interactions
Cell Motility
Anatomical Structure Morphogenesis
Basement Membrane
Extracellular Matrix Organization
Cell Differentiation
Proteosome Degradation
Antigen Processing
mRNA Processing
Complement System

Table S1

Click here to access/download

Supporting Information

Table S1.xlsx

Table S2

Click here to access/download

Supporting Information

Table S2.xlsx

Table S3

Click here to access/download

Supporting Information

Table S3.xlsx

Table S4

Click here to access/download

Supporting Information

Table S4.xlsx

Table S5

Click here to access/download

Supporting Information

Table S5.docx